HHS Public Access

Author manuscript

Cell Rep. Author manuscript; available in PMC 2022 May 11.

Published in final edited form as:

Cell Rep. 2022 April 19; 39(3): 110727. doi:10.1016/j.celrep.2022.110727.

Treg tissue stability depends on lymphotoxin beta-receptor- and adenosine-receptor-driven lymphatic endothelial cell responses

Vikas Saxena[1,2], **Wenji Piao**[1,2], **Lushen Li**[1,2], **Christina Paluskievicz**[1,2], **Yanbao Xiong**[1,2], **Thomas Simon**[1,2], **Ram Lakhan**[1,2], **C. Colin Brinkman**[1,2], **Sarah Walden**[3], **Keli L. Hippen**[3], **Marina WillsonShirkey**[1,2], **Young S. Lee**[1,2], **Chelsea Wagner**[1,2], **Bruce R. Blazar**[3], **Jonathan S. Bromberg**[1,2,4,5,*]

[1]Department of Surgery, University of Maryland School of Medicine, Baltimore, MD 21201, USA

[2]Center for Vascular and Inflammatory Diseases, University of Maryland School of Medicine, Baltimore, MD 21201, USA

[3]Division of Blood and Marrow Transplantation and Cellular Therapy, Department of Pediatrics, University of Minnesota Cancer Center, Minneapolis, MN 55455, USA

[4]Department of Microbiology and Immunology, University of Maryland School of Medicine, Baltimore, MD 21201, USA

[5]Lead contact

SUMMARY

Regulatory T cell (Treg) lymphatic migration is required for resolving inflammation and prolonging allograft survival. Focusing on Treg interactions with lymphatic endothelial cells (LECs), we dissect mechanisms and functional consequences of Treg transendothelial migration (TEM). Using three genetic mouse models of pancreatic islet transplantation, we show that Treg lymphotoxin (LT) αβ and LEC LTβ receptor (LTβR) signaling are required for efficient Treg migration and suppressive function to prolong allograft survival. Inhibition of LT signaling increases Treg conversion to Foxp3^{lo}CD25^{lo} exTregs. In a transwell-based model of TEM across polarized LECs, non-migrated Tregs become exTregs. Such conversion is regulated by LTβR nuclear factor κB (NF-κB) signaling in LECs, which increases interleukin-6 (IL-6) production and drives exTreg conversion. Migrating Tregs are ectonucleotidase CD39^{hi} and resist exTreg conversion in an adenosine-receptor-2A-dependent fashion. Human Tregs migrating across human LECs behave similarly. These molecular interactions can be targeted for therapeutic manipulation of immunity and suppression.

*Correspondence: jbromberg@som.umaryland.edu.

AUTHOR CONTRIBUTIONS

Conceptualization, V.S. and J.S.B.; methodology, V.S. and J.S.B.; investigation, V.S., W.P., L.L., C.P., Y.X., T.S., R.L., C.C.B., S.W., K.L.H., M.W., Y.S.L., C.W., B.R.B., and J.S.B.; writing, V.S. and J.S.B.; funding acquisition, J.S.B.; resources, V.S. and J.S.B.; supervision, J.S.B.

DECLARATION OF INTERESTS

The authors declare no competing interests.

SUPPLEMENTAL INFORMATION

Supplemental information can be found online at https://doi.org/10.1016/j.celrep.2022.110727.

In brief

Saxena et al. show that, to prolong allograft survival, Treg transendothelial migration across LECs is required and involves Treg lymphotoxin (LT) αβ and LEC LTβR signaling. Disrupting LT signaling converts Tregs to non-suppressive Foxp3^{lo}CD25^{lo} exTregs via LTβR-NF-κB-driven IL-6 secretion by LECs. Adenosine-A2AR signaling in LEC promotes Treg stability.

Graphical Abstract

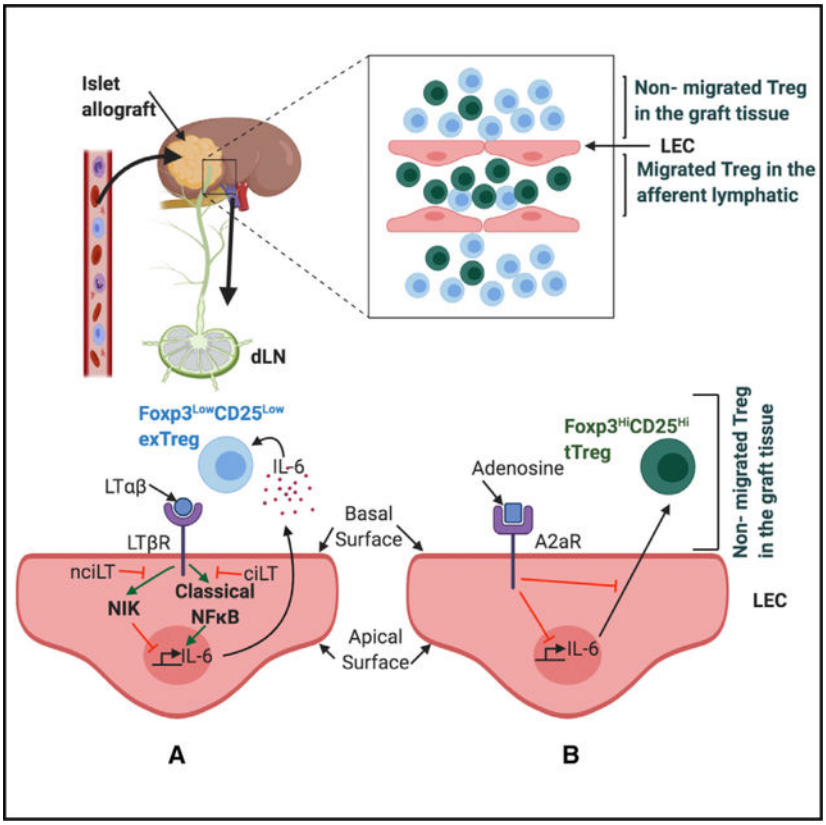

INTRODUCTION

Regulatory T cells (Tregs) are important for immunological tolerance and the resolution of inflammation (Burrell et al., 2012). In transplantation, Tregs must migrate to grafts and lymph nodes (LNs) to promote allograft acceptance (Ochando et al., 2005). In our previous studies, we demonstrated that optimal graft survival is required for Treg migration from blood to pancreatic islet allografts and then to afferent lymphatics and the draining LNs (dLNs) (Zhang et al., 2009). Tregs are also the major lymphocyte subset migrating out of inflamed skin, and this migration is involved in regulating inflammation (Tomura et al., 2010). Thus, Treg migration from blood to tissues to dLNs is important in the resolution of immunity and inflammation. However, the mechanisms that regulate Treg migration from tissues to LNs via afferent lymphatics are not well understood.

The natural thymus-derived Tregs (tTregs) develop from $Foxp3^{-}CD4^{+}CD8^{-}CD25^{+}$ mature thymocytes. In thymus, Treg differentiation requires T cell receptor (TCR) stimulation. In the peripheral tissues, $CD4^{+}CD25^{-}Foxp3^{-}$ conventional T cells, in the presence of high levels of retinoic acid or transforming growth factor β (TGFβ), develop into peripheral Tregs (pTregs). Treg differentiation leads to the upregulation of CD25, allowing IL-2 signaling and Treg transcription factor Foxp3 induction and activity (Lio and Hsieh, 2008). Maintenance of Foxp3 expression is required for ensuring the transcriptional program and the suppressor function of Tregs (Gavin et al., 2007; Lin et al., 2007). At the epigenetic level, three conserved non-coding sequences (CNSs 1–3) in the Foxp3 locus are major determinants of the Treg pool size and Foxp3 stability. The Treg-specific demethylated region (TSDR), containing the demethylated CpG signature of Tregs, is located in the CNS2 region. Loss of Foxp3 expression results in development of exTregs or exFoxp3 Tregs and can be defined as $CD4^{+}CD25^{lo}Foxp3^{lo}$ T cells expressing pro-inflammatory cytokines interleukin-17 (IL-17) and/or interferon gamma (IFNγ) and are hypermethylated at the CNS regions in the Foxp3 locus. ExTregs lose suppressive function and may become pathogenic or induce autoimmunity (Saxena et al., 2021). There is limited knowledge about what factors initiate and drive the exTreg phenotype in general and in the context of transplantation in particular.

Recently, we demonstrated important attributes of Treg migration, which are distinct from non-Treg $CD4^{+}$ T cells (Brinkman et al., 2016). Both tTregs and pTregs have elevated expression of cell-surface lymphotoxin (LT). Tregs use LTαβ to migrate across afferent lymphatics by binding to lymphatic endothelial cell (LEC) LTβ receptor (LTβR). LTαβ-LTβR induces non-classical nuclear factor κB (NF-κB)-inducing kinase (NIK) signaling, which then modulates LEC adhesion molecules, intercellular junctions, and chemokines (Brinkman et al., 2016; Piao et al., 2018, 2019), and conditions LECs for enhanced transendothelial migration (TEM) of other leukocytes toward lymphatic vessels and draining LNs (dLNs) and helps resolution of inflammation (Piao et al., 2020). This distinct form of T cell migration used by Tregs in tissues may serve an essential role in their suppressive physiology.

We previously established that Tregs must migrate through tissues and afferent lymphatics in order to promote transplant survival (Zhang et al., 2009). Because Tregs employ this LT-dependent mechanism for afferent lymphatic migration, we explored the hypotheses that LT regulation of the Treg-LEC interaction is required not only for allograft protection and suppressive function but also for the maintenance of Treg stability.

RESULTS

Treg suppression for islet-allograft protection requires LEC LTβR engagement

We previously demonstrated that Tregs used LTαβ to migrate from the allograft to dLNs and that LT deficiency or blockade on Tregs prevented normal migration and allograft protection (Brinkman et al., 2016). To investigate LTαβ-LTβR interactions for Treg function in islet transplantation, graft survival was measured in the absence or presence of tTregs co-transferred with islets underneath the renal capsule of diabetic recipient mice. Diabetic C57BL/6 recipients transplanted with islets plus local adoptive transfer with $LT\alpha^{-/-}$ tTregs

had an islet graft mean survival time (MST ± SEM) of 13 ± 1.34 compared with 23 ± 2.18 days with the adoptive transfer of wild type (WT) tTregs ($p < 0.001$) (Figure 1A), indicating that LT deficiency in Tregs prevented prolongation of survival.

We also compared islet-allograft survival in LTβR$^{-/-}$ recipients, where LTβR is deleted in the germline. Local transfer of WT tTregs to LTβR$^{-/-}$ recipients did not prolong islet-allograft survival (MST 12.5 ± 1.00 days in LTβR$^{-/-}$ [no tTregs]; 15 ± 0.83 days in LTβR$^{-/-}$ [with tTregs], p not significant [ns]). In contrast, the local transfer of tTregs to WT recipients prolonged islet-allograft survival (12 ± 0.42 [no tTregs] to 23 ± 2.18 days [with tTregs], $p < 0.003$) (Figure 1B). Thus, by using two different genetic-deletion mouse models (LTα$^{-/-}$ tTregs transferred to WT recipients, and WT tTregs transferred to LTβR$^{-/-}$ recipients), the results demonstrated that the interaction of LTαβ on tTregs with LTβR on LECs was required for the optimal suppressive function of tTregs.

Development of Prox1-Cre-ER^{T2}-LTβR$^{fl/fl}$ transgenic mouse line for selective LEC deletion of LTβR

The LTα$^{-/-}$ and LTβR$^{-/-}$ mice have limitations related to developmental and compensatory effects of germline gene deletions. To overcome these systemic defects, we generated a Prox1-Cre-ER$^{T2+/-}$LTβR$^{fl/fl}$ transgenic mouse line, permitting the study of LT-mediated regulation of Treg-LEC interactions and how LTβR acutely regulates Treg migration and function *in vivo*. Murine LECs express high levels of the LEC-specifying transcription factor Prospero-type homeobox (Prox)-1 (Xiong et al., 2017). Therefore, treatment with tamoxifen should deplete LTβR only in LECs. Mice carrying Prox1-Cre-ER^{T2} and LTβR$^{fl/fl}$ transcripts were identified by PCR-based genotyping (Figures S1A and S1B). Prox1-Cre-ER$^{T2+/-}$LTβR$^{fl/fl}$ (knockout [KO]^{fl}) mice were compared with their littermate Prox1-Cre-ER$^{T2-/-}$LTβR$^{fl/fl}$ (WT^{fl}) mice. Stromal cells harvested from peripheral and mesenteric LNs, spleen, and thymus were evaluated for expression of LTβR in LECs (CD45^{-}gp38^{+}CD31^{+}), blood endothelial cells (BECs) (CD45^{-}gp38^{-}CD31^{+}), and fibroblastic reticular cells (FRCs) (CD45^{-}gp38^{+}CD31^{-}) at days 6, 10, and 15 after initiation of tamoxifen treatment (Figures 2A–2C, S1C, and S1D). LTβR was depleted only from LECs of peripheral and mesenteric LNs in KO^{fl} mice; there was no disruption of gene expression in other stromal cell types. ER^{T2}-mediated deletion of the target *Ltbr* gene showed a cumulative effect over time so that by day 10 post tamoxifen treatment, optimum deletion of LTβR in LN LECs was observed. Therefore, further experiments were conducted on or after day 10 after initiation of tamoxifen.

Selective LTβR deletion in LECs does not affect LN architecture

LTβR$^{-/-}$ mice are devoid of Peyer's patches, colon-associated lymphoid tissues, and peripheral LNs. Their spleens are without marginal zones, T/B cell segregation, or follicular dendritic cell networks (Futterer et al., 1998). Therefore, we examined if deletion of LTβR in KO^{fl} mice altered LN architecture. Hematoxylin and eosin staining of LN sections from tamoxifen-treated WT^{fl} and KO^{fl} mice showed no significant difference in the overall architecture (Figure S1E). Further, no significant differences were observed in B and T cell zone segregation or distribution of ERTR7^{+} FRC network over the whole LN (Figure S1F). Deletion of LTβR on LECs had no significant effect on the total stromal cell

percentages of FRCs, BECs, and LECs in mesenteric or peripheral LNs (Figure S1G). The leukocyte fraction of these LNs also remained unaffected, and no significant differences were observed for $CD4^+$, $CD8^+$, $B220^+$, or $CD11b^+$ cells (Figure S1H). Total $Foxp3^+$ Treg (Figure S1I), tTreg ($Foxp3^+Helios^+$), or pTreg ($Foxp3^+Helios^-$) distribution (Figure S1J) remained unaffected by the LTβR deletion in LECs after tamoxifen treatment when analyzed by flow cytometry in various secondary lymphoid organs. Innate lymphoid cell (ILC) populations defined as $lin^-IL\text{-}7R^+Thy1^+$ were analyzed for expression of GATA3 and RORγT. $GATA3^-RORgT^-$ ILC1, $GATA3^+ROR\gamma T^-$ ILC2, and $GATA3^-ROR\gamma T^+$ ILC3 did not differ after deletion of LTβR in LECs of KO^{fl} mice (Figure S1L). These observations demonstrated that deletion of LTβR in KO^{fl} mice did not induce major morphologic or immune abnormalities. Thus, these mice allow for the study of LTβR-mediated regulation of Treg migration and function in an otherwise normal environment.

Selective LTβR deletion in LECs prevents Treg migration from tissues to dLNs

To analyze the consequences of LTβR deletion in LECs, freshly isolated naive CD4 T cells or $Foxp3GFP^+$ tTregs were injected in the hind footpads of WT^{fl} and KO^{fl} mice, and migration to the popliteal LNs was evaluated 16 h later. No significant difference in the migration of naive $CD4^+$ T cells was observed between WT^{fl} and KO^{fl} mice (Figure 2D). However, significant inhibition of tTreg migration in KO^{fl} mice was observed (Figure 2D). Therefore, deletion of LTβR in peripheral tissue LECs prevented tTreg migration through afferent lymphatics and into dLNs.

We next determined if LTβR deletion affected LN residency and egress. Enriched tTregs ($CD4^+Foxp3GFP^+$) and naive CD4 cells were co-transferred intravenously into WT^{fl} and KO^{fl} mice. Eighteen hours later, mice were treated with anti-CD62L monoclonal antibodies (mAbs) to prevent further entry via high endothlieal venules (HEVs), and after an additional 18 h, LNs were analyzed by flow cytometry for the content of the transferred cells, as described previously (Brinkman et al., 2016). The results showed that the ratio of the number of tTregs or naive CD4 cells in WT^{fl} to KO^{fl} mice did not differ (Figure 2E), demonstrating that Treg LN entry from blood, residence, and egress were not regulated by LTβR expression on LN LECs. Taken together, tamoxifen treatment induced deletion of LTβR only in LECs, and deletion affected only tTreg migration from tissues through afferent lymphatics to dLNs.

LTβR deletion in LECs affects expression of molecules important for lymphocyte migration

We analyzed the effect of LTβR deletion from LECs on the expression of chemokines and integrins important in TEM. Immunohistochemistry showed reduced expression of CCL21 in tissue lymphatic vessels (Figure 2Fi) and CCL21 and CXCL12 in LNs (Figures 2Fii, 2Fiii, and 2Fv). There was reduced expression of NIK (Figure 2Fiv) and S1P (Figure 2Fvi) in tissue lymphatic vessels. In contrast, expression of VCAM-1 (Figure 2Fiii), ICAM-1, CCL19 (Figure S1M), CXCL9, and CXCL10 (Figure S1N) remained unaffected. CCL21, but not CCL19, is expressed by LECs, which explains the reduced CCL21 but not CCL19 expression in KO^{fl} mice (Comerford et al., 2013). While flow-cytometric analysis showed no difference in the frequency of tTregs and pTregs in WT^{fl} and KO^{fl} mice (Figures S1I and S1J), immunohistochemical staining indicated deletion of Tregs around the LN cortical ridge

of KO^{fl} mice (Figure S1K). Since CCL21, NIK, S1P, and LTβR are important molecules for Treg migration and distribution in secondary lymphoid organs (Brinkman et al., 2016; Piao et al., 2018), and LTβR deletion inhibited their expression, this shows how interference with the LTβR function reduced Treg migration (Figure 2D) and distribution in LNs (Figures 2F–2Fvii and S1K).

Treg-LTαβ engagement with LTβR on LECs is required for Treg suppression for allograft protection

We compared islet-allograft survival in KO^{fl} and WT^{fl} mice. Local transfer of WT tTregs with islets to WT^{fl} recipients prolonged allograft survival from an MST of 12 ± 0.68 (no tTregs) to 25.5 ± 2.15 (with tTregs) days ($p < 0.001$) (Figure 3A). In contrast, local transfer of tTregs to KO^{fl} mice resulted in no increase in MST (11.5 ± 0.43 [no tTregs] to 13 ± 0.68 days [with tTregs], p ns) (Figure 3A). Thus, our observations in three different genetic-deletion mouse models demonstrated that the interaction of Treg-LTαβ with LTβR on LECs was required for Treg suppressive function for islet-allograft protection.

LTαβ-LTβR is required for Treg migration from tissue to dLNs

tTregs from naive WT or $LT\alpha^{-/-}$ Foxp3GFP mice were adoptively transferred locally with the islets to WT recipients. Four days after transplant and transfer, Tregs were isolated from the islet allografts and dLNs. Commensurate with previous observations (Brinkman et al., 2016), LT-deficient tTregs accumulated in the graft tissues (Figure 3Bii) and migrated less efficiently to the dLNs (Figure 3Biii) compared with their WT counterpart, which migrated successfully to the dLNs (Figure 3Biii). tTregs from naive WT Foxp3GFP mice were co-transferred with the islets to WT^{fl} and KO^{fl} recipients. LTβR deletion resulted in a higher frequency and number of tTregs remaining in the graft in KO^{fl} recipients compared with WT^{fl} (Figure 3C). Together with our observations for the footpad migration assay, where cells were analyzed 16 h after adoptive transfer (Figure 2D), and differences in graft survival (Figures 1A and 3A), these data showed that the LTαβ-LTβR interaction was crucial for tTreg trafficking from graft to dLNs through afferent lymphatics lined with LTβR-expressing LECs. It should be noted that migration to dLNs in $LT\beta R^{-/-}$ recipients could not be performed since these mice lack LNs.

Treg stability depends on LTαβ-LTβR and migration

Foxp3 expression levels in Tregs are linked to suppressor function (Fontenot et al., 2003; Wan and Flavell, 2007). Inflammatory conditions affect Foxp3 expression and modulate plasticity of both tTregs and pTregs (Zhou et al., 2009). However, there has been little exploration of the relationship between Treg migration and Foxp3 expression. Our results showed that in KO^{fl} mice, tTregs migrated less well to dLNs, lymphatics and LNs were defective in important molecules required for Treg migration, and transferred Tregs failed to prolong islet-allograft survival. Similarly, $LT\alpha^{-/-}$ tTregs had no *in vivo* survival defect or *in vitro* suppressive defect (Brinkman et al., 2016) but did not migrate to dLNs and were not protective for graft survival. Therefore, we hypothesized that inhibition of the LTαβ-LTβR interaction affected not only Treg migration but also stability and suppressor function. tTregs from WT or $LT\alpha^{-/-}$ mice were co-transferred with islets and then analyzed for maintenance of tTreg phenotype ($CD25^{hi}Foxp3^{hi}$) or conversion to exTreg phenotype ($CD25^{lo}Foxp3^{lo}$) in

grafts and dLNs 4 days after transplantation (Figure 3D). A higher percentage of WT tTregs maintained the tTreg phenotype, whereas a greater percentage of LTα$^{-/-}$ tTregs became exTregs, exhibiting a trend in the grafts (Figure 3Dii) and highly significant differences in the dLNs (Figure 3Diii). Differences between tTregs and exTregs had a similar trend in the Cre-Lox mice, but the magnitude of change was not as significant as for the LTα$^{-/-}$ (data not shown), likely because the Cre-Lox model takes several days to delete gene expression and less than 100% of LECs are altered. Taken together, the LTαβ-LTβR interaction was required for both tTreg migration as well as for the maintenance of Treg stability.

Migrated tTregs maintain Foxp3 expression

The results showed that deficiency in LTαβ or LTβR expression or LTαβ-LTβR signaling resulted in non-migrated Tregs becoming exTregs and losing their suppressive function. We previously showed that blocking a variety of other Treg ligands or receptors inhibited migration and suppression and resulted in conversion to exTregs (Brinkman et al., 2016; Xiong et al., 2016; Zhang et al., 2009). To study the mechanisms of exTreg formation, we used our *in vitro* model of chemokine-driven T cell migration across polarized LECs (Xiong et al., 2017) and measured Foxp3 and CD25 expression in Tregs that did or did not migrate across the LECs (Figure S2A, and gating strategy in Figure S2B). The results showed that non-migrated Tregs that remained in the upper well of the Boyden chamber had a greater propensity to become exTregs (Figures 4Av and 4B) compared with Tregs that migrated to the lower well (Figures 4Avi and 4C). exTreg conversion required both migration and the presence of LECs, so Tregs placed in the Boyden chamber without LECs (Figures 4Aiii and 4B), or Tregs incubated alone or with LECs but without a Boyden chamber (Figures 4Ai, 4Aii, and 4B), did not preferentially convert to exTregs. exTreg conversion required direct interaction with LECs, as LEC-conditioned medium did not induce conversion (data not shown). Treg expression of CD44, CD69, PD-1, PD-L1, IL-10, perforin, and TGFβ did not change during conversion (Figure S3), showing that there was not simply a global inactivation of the T cells. The exTreg conversion had no impact on T helper type 1 (Th1) (T-bet, IFNγ), Th2 (GATA3), and Th17 (RORγT, IL-17) gene expression (Figure S3) during this short *in vitro* assay, although others have observed such changes over much longer times *in vivo* (Butcher et al., 2016; Komatsu et al., 2013; Li et al., 2016). Conversion to exTregs was not accompanied by differences in cell survival (Figure S4A), showing that cell death did not cause conversion. Since only highly purified, sorted Tregs were used, and since the assays were conducted over 6–16 h, it is very unlikely that the accumulation of exTregs was due to the expansion of a small contaminating population of non-Tregs. There were also no changes in the expression of Helios, so exTregs were not preferentially selected among pTregs or tTregs (Figure S5). These findings were consistent with the *in vivo* data showing an accumulation of Tregs with an increased proportion of exTregs in tissues when migration was blocked (Figure 3).

Centrality of Treg function is defined by the expression of Foxp3, CD25, and Treg-type epigenetic changes (Ohkura et al., 2013). Pyrosequencing analysis revealed that conversion to exTregs was accompanied by increased methylation of *Foxp3* at the Treg-specific conserved CNS2, also known as the TSDR, showing that decreased Foxp3 expression was accompanied by decreased transcriptional accessibility (Figure 4D). Increased methylation

at the *Foxp3* promoter region of exTregs was also observed; however, it was not statistically significant (Figure S6). The non-migrated Tregs also had less suppressive activity, consistent with the *in vivo* data showing that the tissue exTregs did not protect allografts for enhanced survival (Figure 4E).

exTreg conversion relies on classical LTβR NFκB signaling and IL-6 production

Since IL-2 is required for stability of induced Tregs (iTregs) (Chen et al., 2011; Chinen et al., 2016), we determined if conversion to exTregs is due to IL-2 deficiency in the cultures. The addition of graded doses of IL-2 did not prevent tTreg conversion to exTregs (Figures S7A and S7B). Since the lack of migration was associated with exTreg conversion, we tested if chemokine stimulation regulated conversion. However, the addition of CCL19 did not prevent tTreg conversion to exTregs (data not shown). We concluded that exTreg conversion was not regulated by IL-2 or chemokine stimulation.

Since LTβR signaling was required for Treg migration across LECs and exTreg conversion *in vivo*, we determined the role of LEC LTβR on exTreg conversion *in vitro*. We assessed if exTreg conversion was influenced by LTβR decoy peptides (Piao et al., 2018, 2019) that specifically blocked signaling through non-classical NIK (nciLT) or classical (ciLT) NF-κB pathways. Blocking classical, but not non-classical, LTβR NF-κB signaling prevented conversion to exTregs (Figure 5A) in a dose-dependent manner (Figure S8). Since classical NF-κB signaling regulates production of IL-6 by LECs (Xiong et al., 2017), and IL-6 induces exTreg conversion (Garg et al., 2019; Hua et al., 2018), we determined if classical NF-κB signaling was related to IL-6 and if IL-6 was related to exTreg conversion. Neutralization of IL-6 in the cultures with anti-IL-6 mAbs inhibited exTreg conversion (Figures 5B and S4B). An ELISA of supernatants from the upper and lower wells demonstrated substantial quantities of IL-6 produced by LECs, with higher concentrations in the upper wells of the chambers when Tregs were present (Figure 5C). Since the LECs are polarized (Brinkman et al., 2016; Piao et al., 2018; Xiong et al., 2016), these data demonstrated preferential secretion of IL-6 on the LEC abluminal (or basal) surface. Blocking classical, but not non-classical, LTβR NF-κB signaling reduced the quantity of IL-6 produced by LECs (Figure 5D). These actions of decoy peptides and anti-IL-6 were confirmed *in vivo* in the footpad migration assay, where treatment with ciLT or anti-IL-6, but not nciLT, prevented exTreg conversion of non-migrated Tregs in the footpad (Figure 5E and gating strategy in Figure S2B), while no differences were observed in cells that migrated to the popliteal dLNs (Figure S4C). Taken together, we concluded that classical LTβR NF-κB signaling (Brinkman et al., 2016; Piao et al., 2018) resulted in polarized IL-6 secretion by LECs and conversion of the non-migrating Tregs in the upper well *in vitro* or the footpad *in vivo* to exTregs.

We previously showed that murine primary LECs expressed high levels of the LTβR and had constitutive activation of LTβR signaling (Piao et al., 2018). To determine whether LEC LTβR signaling and IL-6 secretion were stimulated by Treg LTαβ, we compared exTreg conversion in WT and $LT\alpha^{-/-}$ Tregs. Similar to WT tTregs, a high percentage of non-migrated $LT\alpha^{-/-}$ tTregs became exTregs *in vitro* (Figure 5G) and *in vivo* (Figures 5F and S4D). $LT\alpha^{-/-}$ tTregs stimulated IL-6 secretion by LECs, and anti-IL-6 mAbs inhibited

exTreg conversion (Figures S4E and S4F) and IL-6 accumulation (Figure S4G). Taken together, these results showed that direct LTβR stimulation of LECs by Tregs was not required for IL-6 secretion and exTreg conversion, suggesting either constitutive LTβR activation and/or that stimulation of LTβR signaling was regulated by additional interactions with WT or $LT\alpha^{-/-}$ Tregs.

Adenosine prevents exTreg conversion

The migrated and non-migrating cells were assessed for the expression of other important molecules (Figures 6A and S3). Compared with non-migrating Tregs, those that migrated had higher expression of CD39 and biphasic expression of CD73, both ectonucleotidases important for generating extracellular adenosine and required for Treg suppressive function (Sauer et al., 2012). In AMP-Glo assays, Tregs had both CD39 and CD73 enzymatic activity (Figure 6B). Treg interaction with murine LECs (mLECs) induced CD73 activity in both the migrated and non-migrated Tregs but reduced CD39 ectonucleotidase activity in the non-migrated cells of the upper chamber. Interestingly, Treg interaction directly with LECs (without transwell [TW]) induced CD73 activity but reduced CD39 activity significantly(Figure 6B). These results suggested that the non-migrated Tregs had less ectonucleotidase activity compared with the migrated Tregs.

Available antibodies against CD39 and CD73 only weakly inhibited ectonucleotidase activities (data not shown), thus the precise role of these molecules in exTreg conversion could not be directly established by antibody blockade. Although extracellular adenosine levels in the culture supernatants remained unchanged (Figure S9A), the addition of adenosine to culture or to the footpad assay prevented exTreg conversion (Figures 6C–6E and S4H–S4J), while adenosine had no significant effect on Treg migration (Figure S9B). Using pharmacological inhibitors, adenosine-mediated rescue of exTreg conversion was specifically inhibited by blocking the A2aR (high affinity) but not the A2bR receptor on LECs in both the transwell and footpad migration assays (Figures 6D, 6E, S4I, and S4J). Additional specificity experiments determined that LEC pre-treatment with adenosine, but not Treg pre-treatment, rescued exTreg conversion (Figures 6J, S4K, and S9C).

Adenosine pre-treatment had no effect on LEC morphology but acutely regulated LEC structure and integrity, inducing junctional accumulation of VCAM-1 and zonulin-1 (ZO-1) (Figures 6F and 6G). Adenosine also enhanced lymphatic permeability, as shown by dye transport across the LEC monolayer (Figure 6H) and from tissues to dLNs (Figure 6I), in an A2aR-dependent manner.

The effects of adenosine on preventing exTreg conversion correlated with decreased IL-6 levels in the cultures (Figures 6K, S4L, and S9D), and adenosine-mediated rescue of exTreg conversion was inhibited by adding exogenous IL-6 (Figures 6L and S4M). The nciLT, but not ciLT, decoy peptides inhibited adenosine-mediated rescue of tTreg conversion to exTregs (Figures 6M and S4N) by increasing IL-6 secretion (Figures 6N and S4O). Adenosine did not act through LTβR pathways, since Treg stimulated NIK and classical NF-κB activity in LECs, as we previously showed (Piao et al., 2018), but adenosine did not alter these activities (Figures S9E and S9F). Neither IL-6 nor LTβR signaling blockers altered adenosine levels in the supernatants (Figure S9G). Together, we concluded that

adenosine-mediated rescue of exTreg conversion was due to altered endothelial structure and permeability, thereby changing IL-6 distribution.

Finally, we confirmed that human Tregs migrating across human LECs underwent exTreg conversion (Figures 7A, 7B, and S10A), and polarized IL-6 secretion was observed (Figure 7C). LTβR decoy peptides, adenosine, and anti-IL-6 mAbs inhibited exTreg conversion (Figures 7D, 7E, and S10B). Anti-IL-6 was the most potent inhibitor, while the other reagents exhibited variable inhibition, likely reflecting the heterogeneity among different human donor samples.

DISCUSSION

We established a conditional LTβR$^{-/-}$ mice model (KO^{fl}) in which LTβR transcripts were selectively depleted from LECs. In KO^{fl} mice, LN architecture, distribution of LN stromal cells (LNSCs), and leukocyte and ILC subset percentages remain unchanged. Nonetheless, LTβR deletion inhibited Treg migration from tissues to dLNs, although Treg egress from the LNs was not affected. LTβR deletion in LECs reduced expression of chemokines and cell adhesion molecules in tissues and LNs and inhibited accumulation of Tregs in the cortical ridge of the LNs. We previously demonstrated that LNSCs, which include LECs, construct specific niches in the LNs to regulate immunity. In particular, the distribution of Tregs around the LN HEVs and cortical ridge is dependent on several signals and is important for inducing and maintaining suppression and tolerance (Li et al., 2020). The interaction of Treg LTαβ with LTβR on LECs is important for Treg migration from tissues to afferent lymphs and then to LNs (Brinkman et al., 2016; Piao et al., 2018). Treg signaling enhances LEC permissiveness for Treg and other leukocyte TEM and induces expression of molecules, such as CCL21 and VCAM-1, important for Treg migration (Piao et al., 2020). LNSCs produce stromal laminin α5 fibers, which regulate expression of chemokines and cell adhesion molecules, and are important for Treg migration and distribution in the LNs (Li et al., 2020; Saxena et al., 2019; Simon et al., 2019). Taken together, these data showed that deletion of LTβR on LECs resulted in decreased LEC permissiveness for TEM and decreased expression of chemokine and adhesion molecules functionally important for the peripheral tissue and LN microenvironments. These tissue and LN alterations resulted in reduced Treg migration and distribution within LN microdomains required for immune regulation.

How Tregs are regulated to migrate to and function in a particular environment or tissue is not well understood. We previously showed that sequential Treg migration from blood to grafts to afferent lymphatics and dLNs is important for the suppression of alloimmunity and for allograft survival (Zhang et al., 2009). By using three different genetic-deletion models, we showed here that the interaction between Treg LTαβ and LEC LTβR was important for Treg migration as well as prolongation of allograft survival. While Tregs migrating to the dLNs were strongly associated with allograft protection, non-migrated Tregs, unable to interact with LEC LTβR, were retained in the allograft. Retained Tregs were more likely to be converted to Foxp3^{lo}CD25^{lo} exTregs, which lacked regulatory function (Gavin et al., 2007; Lin et al., 2007). These results demonstrate that the importance of migration of Tregs in maintaining suppressive function is linked to their stability versus conversion to

exTregs. These results suggest that for therapeutic purposes, Tregs must maintain LTαβ expression and other cellular machinery required for migration between peripheral and lymphoid tissues.

Treg stability is regulated by a number of factors, and Tregs lose their identity upon loss of Foxp3 expression (Williams and Rudensky, 2007), often resulting in severe inflammatory disorders (Zhou et al., 2009). However, the proximal signals responsible for determining Treg instability are not well defined. To study the mechanisms of Treg conversion to exTregs, we successfully adopted our transwell-based *in vitro* assay (Figure S2). This model system demonstrated that following interaction with LECs, the migrated Tregs profoundly changed their phenotype compared with non-migrated Tregs. Migrated Tregs expressed higher levels of CD39, CD73, CTLA4, GITR, and LTαβ, they were more demethylated at both the *Foxp3* promoter and the TSDR region, and they more efficiently suppressed T cell proliferation. Thus, Treg TEM across LECs was an active process that helped Tregs maintain or acquire characteristics important for suppressive function. The utility of our *in vitro* model can be enhanced by incorporating other cell types and stromal elements.

In lymphopenic hosts lacking conventional T cells, adoptive transfer of purified $Foxp3^+$ Tregs results in exTreg conversion (Duarte et al., 2009; Komatsu et al., 2009; Zhou et al., 2009). In addition, use of fate-mapping models shows that some exTregs can be traced back to activated T cells transiently expressing Foxp3 (Miyao et al., 2012). In contrast, Rubtsov et al. (2010) and Junius et al. (2021) found that $Foxp3^+$ tTregs represent a stable cell lineage. Thus, the development of exTregs is still a controversial issue, and great care must be taken to use highly purified and well-defined subsets, as in our present investigations. Treg development and function depend not only on the Foxp3 expression but also require CD25 expression and changes in the epigenome (Ohkura et al., 2013). For true Tregs, the molecular mechanisms governing loss of Foxp3 are complex (reviewed in Saxena et al., 2021). We deciphered mechanisms involved in Treg conversion to exTregs and identified approaches to rescue this conversion. IL-6 is known to drive exTreg conversion (Garg et al., 2019; Hua et al., 2018) and regulate the Th17/Treg balance by suppressing Treg generation and inducing Treg instability (Joller and Kuchroo, 2014). We showed that LECs secreted IL-6 in response to LTβR classical NF-κB stimulation. IL-6 secretion was polarized and accumulated preferentially in the abluminal (basal) or tissue side of the LECs. Blocking classical NF-κB signaling or inhibiting IL-6 with blocking mAbs prevented exTreg conversion. Since our previous studies showed that Treg LTαβ primarily stimulated LEC LTβR-NIK signaling, the current results suggest that more prolonged interactions of LECs with non-migrating Tregs may preferentially induce LTβR-NFκB signaling. While we primarily examined the LT system in these interactions, both the WT and $LT\alpha^{-/-}$ Tregs converted to exTregs to a similar extent, suggesting that other mechanisms also regulate NIK and NF-κB, such as strong inflammation that results in the production of IL-6.

We also identified adenosine as a factor contributing to the maintenance of Treg phenotypes. A2aR stimulation can induce Treg proliferation and stronger immunosuppression (Ohta et al., 2012); however, its role in Treg stability and migration has not previously been explored. Tregs convert extracellular nucleotides into pericellular adenosine through CD39/CD73 ectonucleotidase activities. Adenosine stimulates A2aR on T cells and inhibits

expression of NF-κB-regulated cytokines that may impair Treg function or stability, such as IL-2, TNFα, IFNγ, and IL-6 (Ohta et al., 2012; Romio et al., 2011; Zarek et al., 2008). In experimental autoimmune uveitis, Treg emergence and stability depends on A2aR stimulation (Muhammad et al., 2020). In patients with systemic lupus erythematosus, A2aR activation inhibits classical NF-κB and reduces inflammatory cytokines including IL-6 (Bortoluzzi et al., 2016), and an A2aR agonist reduces IL-6 and increases Tregs (Zheng and Wang, 2020). In osteoblastic cell lines, A2aR stimulation has been shown to inhibit IL-6 secretion (Russell et al., 2007). Thus, the CD39-CD73-adenosine axis comprises an important component of Treg stability and suppressive machinery. LECs from afferent lymphatics express CD73 (Algars et al., 2011), although the role of CD73 on LECs in lymphatic migration has not been reported. LECs also express A2aR and A2bR, and blockade of A2aR signaling impairs capillary-like tube formation, which is partly restored by exogenous adenosine (Allard et al., 2019). We showed here that migrated Tregs expressed more CD39, and the addition of adenosine altered LEC permeability and junctional structure and inhibited Treg conversion to exTregs. Treg interaction with LECs reduced CD39 ectonucleotidase activity in non-migrated Tregs while enhancing CD73 activity (Figure 6B). Since adenosine generation is mediated by both CD39 (catalyzing ATP/ADP to AMP) and CD73 (catalyzing AMP to adenosine), a decrease in CD39 activity will result in less AMP available for enhanced CD73 activity and will thus be unable to rescue Tregs. This suggests that non-migrated Tregs in proximity to LECs may not be able to convert ATP to AMP and thus adenosine. It may also explain that the addition of exogenous adenosine, but not available ATP, rescues Treg conversion and that A2aR antagonists alone do not enhance Treg conversion since adenosine already seems to be limiting. $CD39^{hi}$ Tregs have been shown to be more stable under inflammatory conditions (Gu et al., 2016). Since agonists of adenosine receptors are currently being evaluated in clinical trials for diverse diseases, they could be explored for their role in Treg function and stability (Jacobson et al., 2019). Taken together, our results suggest that Treg-LEC interactions stimulate both classical and non-classical NF-κB activity, adenosine generation and IL-6 secretion and guide Treg migration where migrated Tregs are stable. However, we have not explored role of other variables such as inflammation, interaction with other cells, or the myriad of other receptors and ligands known to be expressed by these cells. Based on our observations, we propose that the Treg-LEC interaction engages LTαβ-LTβR, which induces IL-6 secretion. Since the addition of adenosine rescues Treg conversion via A2aR and LECs inhibit Treg CD39 activity, the adenosine generated even by an enhanced CD73 ectonucleotidase activity may not reach the threshold to bypass the effects of IL-6, which results in Treg conversion to exTregs.

The stochastics of exTreg conversion could be due to several factors. Tregs are heterogeneous, with graded expression of different transcription factors, including Foxp3. Thus, some Tregs may be pre-determined to become exTregs, while others are better at maintaining the Treg phenotype. Another non-mutually exclusive explanation is that the intensity and affinity by which Tregs interact with LECs determine their fate (Bailey-Bucktrout et al., 2013). In our *in vitro* transwell-based assay, the sorted Tregs were selected for Foxp3 expression, and we did not differentiate whether they were of thymic origin or peripherally iTregs, although in young unmanipulated mice, they were mostly likely to

be tTregs (Petzold et al., 2014). We and others (Lam et al., 2021) noted that differences in expression of Helios did not correlate with exTreg conversion or stability (Figure S5). Exploration of these possibilities may help Treg-based therapies to lock in the Treg phenotype so that stabilized cells will not change following antigen-driven activation or in inflammatory environments. Such approaches will limit Tregs converting to exTregs and prevent autoimmune effector T cell development.

Overall, our study provided details of Treg-LEC interactions that regulated Treg migration across LECs and mechanisms behind ill-fated non-migrated exTreg conversion. exTregs are pathogenic in various disease models, including arthritis, colitis, corneal transplantation, experimental autoimmune encephalitis, lung and liver inflammation, and type 1 diabetes (Guo and Zhou, 2015). exTreg conversion also poses a significant hurdle in the development of Tregs as a cellular immunotherapy. The targets we identified provide tools for the development and control of Tregs as an effective method of cellular immunotherapy and as approaches for augmenting or inhibiting Treg function *in vivo* for diverse immune-mediated diseases.

Limitations of the study

Our study shows that Treg-LEC interactions regulate Treg migration and stability. We showed a role for Treg-LTα-LTβR-LEC, CD39/CD73/adenosine/A2aR, and IL-6. However, we have not tested the effects of other Treg-LEC receptor-ligands pathways. Since adenosine and/or anti-IL-6 did not completely rescue exTreg conversion, we predict there are additional elements responsible. Since we demonstrated the non-migrated Tregs were more likely to be converted to exTregs, fate-mapping methods could establish if Treg fitness determines trafficking and fate or if migrated Tregs acquire better fitness during migration. Our analyses were directed against Treg-LEC interactions. However, the physiological relevance of these molecules during Treg interactions with other stromal cells, such as FRCs and BECs, needs further exploration. We are developing a mouse model of Tregs devoid of IL-6 receptors and performing metabolomic screens of Tregs to explore additional factors.

STAR★METHODS

RESOURCE AVAILABILITY

Lead contact—Further information and requests for resources and reagents should be directed to and will be fulfilled by the Lead Contact, Jonathan S. Bromberg (jbromberg@som.umaryland.edu).

Materials availability—All mice lines and generated materials in this study are available from the lead contact with a completed materials transfer agreement.

Data and code availability

- All data reported in this paper will be shared by the lead contact upon request.
- This paper does not report original code.

- Any additional information required to reanalyze the data reported in this paper is available from the lead contact upon request.

EXPERIMENTAL MODEL AND SUBJECT DETAILS

Mice—LTβR$^{fl/fl}$ mice were from Thomas Helgans (University of Regensburg, Regensburg, Germany) (Wimmer et al., 2012), and Prox1-Cre-ER^{T2} Tg mice were from Guillermo Oliver (St. Jude Children's Hospital, Memphis, TN) (Srinivasan et al., 2007). Mice were crossed for three generations to generate Prox1-Cre-ER^{T2}-LTβR$^{fl/fl}$ mice. Mice were kept heterozygous for Cre-ERT2 by backcrossing homozygous Prox1-Cre-ER$^{T2+/-}$LTβR$^{fl/fl}$ mice with C57BL/6. PCR based genotyping used primers for LTβR: 5′-GAA GCA TAG CATTGT CCC ACG G-3′ (forward) and 5′-CTA TGA GGC AAT GGG GAA AGA GGG-3′ (reverse); and for Prox1Cre: 5′- TGT CTG TGC CTC CAT CTC AG −3′ (forward) and 5′-AGG CAA ATT TTG GTG TAC GG-3′ (reverse). Foxp3GFP (Fontenot et al., 2005) mice on a C57BL/6 background were from Alexander Rudensky (Memorial Sloan Kettering Cancer Center, New York City, NY). C57BL/6 and LTα$^{-/-}$ mice were purchased from The Jackson Laboratories (Bar Harbor, ME). LTα$^{-/-}$ mice were crossed with Foxp3GFP mice to generate LTα$^{-/-}$ Foxp3GFP mice. For *in vivo* migration studies in WT^{fl}, KO^{fl}, B6, and LTβR$^{-/-}$ mice (all CD45.2^{+}), CD45.1^{+}Foxp3GFP^{+} mice were used for sorted tTregs. To compare migration of WT vs LTα$^{-/-}$ tTregs, CD45.1^{+} recipient mice were used. WT^{fl} and KO^{fl} mice were injected with tamoxifen (Sigma-Aldrich, St. Louis, MO) (125 mg/kg body weight i.p. suspended in corn oil) for five consecutive days. All recipient mice were injected with streptozotocin (180 mg/kg body weight i.p.) for diabetes induction. Tamoxifen treated mice were rested for at least 10 days after the final injection to minimize toxicity, and then given streptozotocin. All animal experiments were performed with age- and sex-matched mice in accordance with Institutional Animal Care and Use Committee approved protocols.

METHOD DETAILS

Cells—C57BL/6 mouse primary dermal LECs (C57-6064L) and human LEC (H-6064L) were from Cell Biologics, Inc. (Chicago, IL) and cultured according to the manufacturer's instructions in manufacturer-provided mouse or human endothelial cell medium, respectively, supplemented with 5% fetal bovine serum (FBS), 2mM L-glutamine, 100 IU/mL penicillin, vascular endothelial growth factor, endothelial cell growth supplement, heparin, epidermal growth factor, and hydrocortisone. For mouse T cell purification and culture, CD4^{+} T cells were first enriched by magnetic bead negative selection (Stemcell Technologies, Vancouver, Canada), and then sorted using FACS Aria II (BD Bioscience, Franklin Lakes, NJ) for CD4^{+}FoxP3GFP^{+} tTregs and CD4^{+}CD44^{lo}CD25^{-}FoxP3^{-} naïve CD4 from FoxP3GFP WT or FoxP3GFP LTα$^{-/-}$ mice. Cell purity was always >98%. Naïve human Treg (CD4^{+}CD25^{hi}CD127^{-}CD45RA^{+}) were sorted from peripheral blood mononuclear cells. The sorted cells were incubated with an irradiated K562 cell line engineered to express CD86 and the high-affinity Fc Receptor (CD64) (KT86/64) as previously described (Hippen et al., 2011). Cells were cultured in XVivo-15 medium (Lonza, Walkersville, MD) containing 10% human AB serum (Valley Biomedical, Winchester, VA), Pen/Strep and GlutaMAX (Invitrogen, Carlsbad, CA), N-acetyl cysteine (USP), and recombinant human IL-2 (300 IU/mL; Chiron, Emeryville, CA). After 14 days, cells were assayed with the *in vitro* LEC co-culture.

Peptides—LTβR decoy peptides synthesis and usage were described previously (Piao et al., 2019).

Stromal cell isolation—Stromal cells were isolated by enzymatic digestion of pooled LNs, spleen, and thymus following the protocol as described by Fletcher et al. (Fletcher et al., 2011). Tissues were digested with 2 mL of freshly made enzyme mix comprised of RPMI-1640 containing 0.8 mg/mL dispase (Gibco, Gaithersburg, MD), 0.2 mg/mL collagenase P (Roche, Basel, Switzerland), and 0.1 mg/mL DNase I (Invitrogen, Carlsbad, CA). Isolated cells were resuspended in 10 mL MACS buffer (2% FBS, 1mM EDTA, and 1x PBS), filtered through 70 μm nylon mesh, counted, and assessed for viability using trypan blue.

Flow cytometry—Cells harvested from different organs were made into single cell suspensions and incubated in flow cytometry staining (FACS) buffer containing phosphate-buffered saline (PBS) containing 0.2 mM calcium, 0.1 mM magnesium, and 0.5% fetal calf serum. Cells were treated with anti-CD16/32 (clone 93, eBioscience) to block Fc receptors, and stained with antibodies to cell surface molecules, as indicated in key resources table. Stained cells were analyzed by flow cytometry using a BD LSR-Fortessa X20 cytometer (BD Biosciences, San Jose, CA). Results were analyzed with FlowJo v9.9.6 (TreeStar, Ashland, OR). Quantitative differences are expressed as geometric mean fluorescence intensity (gMFI) of cells minus isotype IgG gMFI. Staining for Annexin V and 7-AAD was performed using PE Annexin V apoptosis detection kit (BD Biosciences, San Jose, CA).

Immunohistochemistry and histology—LNs and spleens were fixed in 10% buffered formalin and embedded in paraffin. Sections were cut at 5μm and stained with H&E. For immunohistochemistry, organs were frozen with OCT compound (Scigen Tissue-Plus, Gardena, CA). Frozen sections were cut at 6μm, fixed with cold acetone, blocked with 5% goat or donkey serum (Jackson ImmunoResearch, West Grove, PA) and incubated with the indicated antibodies (Key resources table). For pinna whole mounts, ears were depilated, peeled into 2 pieces, and fixed with 4% paraformaldehyde (PFA) for 15 minutes at room temperature. Samples were further processed as described previously (Brinkman et al., 2016; Piao et al., 2018). LEC monolayers were stained as described previously (Xiong et al., 2017). Images were acquired with a Nikon Eclipse 700 (Nikon, Melville, NY, USA) and analyzed with Volocity image analysis software (Perkin Elmer, Waltham, MA). The positive staining area percentage was quantified based on at least three independent experiments with 3 mice/group, 3 LN/mouse, 3 sections/LN, 3–5 fields/section.

Footpad migration assay—Freshly sorted $CD4^+FoxP3GFP^+$ tTregs from FoxP3GFP mice and $CD4^+CD44^{lo}CD25^-FoxP3^-$ naïve CD4 from FoxP3GFP CD45.1 mice were used. Mice were anaesthetized with ketamine (80–100 mg/kg ip) and xylazine (8–10 mg/kg ip) and 1×10^6 tTregs or naïve $CD4^+$ non-Tregs were injected into the hind footpads in 20 μL 1x PBS. Popliteal dLN and/or footpad tissues were collected 16 hours post injection and processed for flow cytometry (Brinkman et al., 2016). For exTreg assay, non-migrated Tregs were harvested in FACS buffer from the triturated footpad.

LN egress assay—LN egress of T cell was performed as described previously (Brinkman et al., 2016). $CD4^+$ T cells were purified from FoxP3GFP CD45.1 mice with magnetic bead negative selection (Miltenyi, Auburn, CA). 2×10^7 cells were injected i.v. into tamoxifen treated WT^{fl} or KO^{fl} mice ($CD45.1^-$). After 18 hours, 100 μg anti-CD62L (MEL-14, BioXCell) or control Rat IgG2a (2A3, BioXCell) was injected i.v. After another 18 hours, LNs were collected for each group and analyzed by flow cytometry for transferred naïve $CD4^+$ T cells ($CD45.1^+Foxp3^-$) and tTregs ($CD45.1^+Foxp3^+$). The numbers and ratios of transferred naïve CD4 T cells or tTregs in WT^{fl} and KO^{fl} LN were calculated.

Murine islet isolation and transplantation—Murine islet isolation and transplantation was performed as previously published (Brinkman et al., 2016). Blood glucose <150mg/dL after transplantation was considered engraftment, and >300mg/dL was considered diabetic or graft rejection as appropriate. Blood glucose was measured via tail nicking with a handheld meter (TRUEtrack, TRIVIDIA Health, Fort Lauderdale, FL, USA).

Identification of innate lymphoid cells (ILCs)—ILCs were identified as described previously (Yang et al., 2018). Briefly, a LN single cell suspension was prepared by passing cells through 70 μm nylon mesh strainer. Lineage (Lin) negative cells were analyzed for the IL-7Rα and Thy1 expression. Dump channel for lineage contained antibodies against CD3e, TCRβ, GL3, CD19, GR1, CD11b, CD11c, F4/80, Ter-119, NK1.1, and CD49b. $Lin^-IL\text{-}7R\alpha^+Thy1^+$ cells were analyzed for the expression of transcription factors GATA3 and RORγT. ILC subsets were identified as ILC1 ($GATA3^-ROR\gamma T^-$), ILC2 ($GATA3^+ROR\gamma T^-$), and ILC3 ($GATA3^-ROR\gamma T^+$).

Transendothelial migration and tTreg conversion to exTreg assay—Transmigration across LEC was described previously (Piao et al., 2019; Xiong et al., 2017). Briefly, the inverted transwell insert (24-well; Corning Inc., Corning, NY) with 5 μm pore size was coated with 0.2% (w/v) gelatin (Bio-Rad, Hercules, CA) for 1 hour at 37 °C before loading with 1.0×10^5 primary skin LEC in 100 μL mouse endothelial cell medium (Cell Biologics, Inc.). One day later, the LEC cell layers or freshly sorted tTregs were treated with various conditions as noted in the text and figure legends. 2×10^5 treated or non-treated tTregs in 100 μL were loaded into the upper well of the Boyden chamber while the lower chamber contained mCCL19 (50 ng/mL, R&D Systems, Minneapolis, MN). All cells or reagents were prepared in IMDM containing transferrin (Gibco, Gaithersburg, MD) and 0.5% (w/v) fatty acid-free BSA (Gemini, Sacramento, CA). The Tregs were permitted to migrate at 37 °C. For TEM assay, cells that migrated to the lower chamber after 3 hours were counted. For exTreg assay, cells from the upper and lower chambers were analyzed after 16 hours by flow cytometry. Gating strategy is described in Figure S2B. LEC were pretreated with decoy peptide for 30 min at 37°C and washed twice with 1x PBS. LEC or Treg pretreatment with indicated antibodies was performed for 30 min at 4°C, followed by washing twice with 1x PBS. Cultures were incubated with anti-IL-6 or adenosine (TOCRIS, Bristol, UK) at indicated doses. Pharmacological inhibitors of adenosine receptor 2A, (CPI 444) (Enzo, Milpitas, CA) and 2B (MRS 1754) (Sigma-Aldrich, St. Louis, MO) were added at 1μM.

Pyrosequencing—For methylation analysis, cells from male mice were used to avoid artificial recalculation because of X-chromosome inactivation in female mice. FACS-sorted Foxp3GFP^{+} Tregs were co-cultured with LEC for exTreg assay. Tregs were permitted to migrate for 16 hours at 37°C, and then Tregs from the upper and lower chambers were sorted for tTregs (Annexin-V^{-} 7-AAD^{-} CD4^{+} Foxp3GFP^{hi} CD25^{hi}) and exTregs (Annexin-V^{-} 7-AAD^{-} CD4^{+} Foxp3GFP^{lo} CD25^{lo}). FACS-sorted Tregs and Tconv cells were used as controls. Bisulfite-converted DNA was prepared from sorted cells according to the manufacturer's instructions (EZ DNA Methylation-Direct™ Kit, Zymo Research, Irvine, CA). Foxp3 promoter and TSDR regions were amplified by PCR containing 10 ng of bisulfite converted genomic DNA, 1 U Hot Start Taq DNA Polymerase (New England BioLabs, Ipswich, MA), Hot Start Taq PCR buffer, 1μM biotinylated primer and 2μM non-biotinylated primer in a final volume of 50μL reaction (cycle: 95 °C for 15 min; 50× 95°C for 30 s, 47°C for 1 min, 72°C for 1 min; 72°C for 10 min).
The PCR product was analyzed by gel electrophoresis for quality. Then, 3–10μL of the PCR product, Pyromark Gold Q96 reagents, PyroMark Q96 HS plate, Pyromark buffers (Qiagen, Germantown, MD), Streptavidin Sepharose High Performance (GE Healthcare, Chicago, IL), and sequencing primers (IDT, Coralville, IA) were used for pyrosequencing on a PyroMark Q96MD instrument according to the manufacturer's protocol. Methylation was analyzed using CpG SW 1.0.11 software. Amplification and sequencing of the Treg cell-specific demethylated region (TSDR) (chromosome position X:7583986-7584149), the Foxp3 promoter (chromosome position X7579550-7579731) was performed with the following amplification/sequencing primer sets: mTSDR-for, 5′ biotinylated-TAA GGG GGT TTT AAT ATT TAT GAG GTT T 3'; mTSDR-rev, 5' CCT AAA CTT AAC CAA ATT TTT CTA CC 3′; mTSDR-S1, 5′ ACC CAA ATA AAA TAA TAT AAA TAC T 3′; mTSDR-S2, 5′ ATC TAC CCC ACA AAT TT 3′; mTSDR-S3, 5′ AAC CAA ATT TTT CTA CCA TT 3′; mTSDR-S4, 5′ CCA TAC AAA ACC CAA ATT C 3′; mFoxp3 promoter-for, 5′ GGT GAG GGG AAG AAA TTA TAT TTT TAG 3′; mFoxp3 promoter-rev, 5′ biotinylated-TAC CAC ATT ATC AAA AAC AAC TTT ACT T 3′; mFoxp3 promoter-S1, 5′ AAA AAA ATT GGA TTA TTA GAA GAG 3′; mFoxp3 promoter-S2, 5′ ATC AAA AAC AAC TTT ACT TTT ATA C 3′; mFoxp3 promoter-S3, 5′ AGA AGA GAG AGG TTT G 3′. The indicated chromosome positions refer to genome assembly GRCm38.p5.

IL-6 ELISA—The exTreg assay was set up, as described above. Supernatants from upper and lower wells of the exTreg assay were harvested and cleared of cells and debris by centrifugation. Cleared supernatant was stored at −80 °C. Mouse and human IL-6 were measured with ELISA kits from Biolegend (Biolegend, Inc., San Diego, CA), following manufacturer's protocol.

AMP-Glo assay—The exTreg assay was conducted as described above. Cells from upper and lower wells of the exTreg assay, or Treg alone or Treg co-cultured with mLEC (no TW) were harvested. To test function of CD39 ectonucleotidase activity, ATP (25μM) conversion to AMP was measured. To test function of CD73 ectonucleotidase activity, AMP (25μM) depletion (conversion to adenosine) was assessed. Measurements were performed by

following manufacturer's instructions in a luminescence-based AMP-Glo assay (Promega; Madison, WI, USA).

Adenosine estimation—Supernatants from upper and lower wells of the exTreg assay were harvested and cleared of cells and debris by centrifugation. Cleared supernatant was stored at −80 °C. Adenosine was measured with adenosine assay kit (Abcam, Cat# ab211094; Cambridge, MA), following the manufacturer's protocol.

Microsuppression assay—FACS-sorted Foxp3GFP$^+$ Tregs were co-cultured with LEC for the exTreg assay, as described above. Tregs were permitted to migrate for 16 hours at 37 °C, and then Tregs from the upper and lower chambers were sorted (Annexin-V$^-$7-AAD$^-$CD4$^+$Foxp3GFP$^+$). FACS-sorted Tregs, cultured without LEC, were used as controls. eFluor-670 (Molecular Probes, Eugene, OR) labeled responder CD4$^+$ cells (4×10^3) and different numbers of Tregs (ratios of 1:1–1:8, Treg:Teff, 500–4000 Tregs) were activated with Dynabeads (Gibco, Cat# 11452D, Waltham, MA) at a concentration of 1:4 beads:cells. Cells were cultured in a 96-well round bottom plate with 100 μL RPMI for 3 days. Cells were acquired by flow-cytometry and the division index of responder cells was analyzed by measuring relative eFluor 670 dilutions.

Immunoblotting—LECs were washed twice with ice-cold 1x PBS. Cells were lysed and immunoblotting was performed as described previously (Piao et al., 2018).

Dye permeability assays—For *in vivo* permeability, A2aR blocker CPI-444 (1 μM) was injected into hind footpads; 1 hour later, adenosine (10 μM) was injected. 4 hours after adenosine treatment, 30μL Evans Blue (0.67 mg/mL; Sigma-Aldrich, St. Louis, MO) in PBS was administered. Popliteal dLN were collected 16 hours later and dissociated in PBS. Absorbance at OD 620 nm was measured in a microplate reader (TECAN, San Jose, CA).

QUANTIFICATION AND STATISTICAL ANALYSIS

Empirical methods were used to determine sample and experiment size for sufficient statistical power. No samples were excluded specifically from analysis. Survival curves were analyzed according to the Kaplan–Meier estimator, and the difference between two groups was determined by the log-rank (Mantel–Cox) test. Log-rank, two-tailed Student's t-tests, parametric unpaired t test with Welch's correction, and one-way analysis of variance with Tukey were performed using Graphpad software (Prism v9.0). For multiple comparisons, Tukey post tests were used when all possible comparisons were logically meaningful. A p value of <0.05 was considered significant for one-way analysis of variance and t-tests, and for multiple comparisons significance level was adjusted for the number of comparisons being made by the software. Statistical analysis was performed on groups with similar variance. Error bars in figures and value ranges given in the text are mean ± SD unless otherwise noted.

Supplementary Material

Refer to Web version on PubMed Central for supplementary material.

ACKNOWLEDGMENTS

This work was supported by NIH grants 1R01AI114496, 1P01AI153003, and R37AI062765 (J.S.B.) and the Maryland Living Legacy Foundation (J.S.B. and W.P.). We are thankful to the staff of the Malaria Research Center at University of Maryland School of Medicine for help in pyrosequencing. We are also thankful to University of Maryland Greenebaum Comprehensive Cancer Center Flow Cytometry Shared Service for cell sorting.

REFERENCES

Algars A, Karikoski M, Yegutkin GG, Stoitzner P, Niemela J, Salmi M, and Jalkanen S (2011). Different role of CD73 in leukocyte trafficking via blood and lymph vessels. Blood 117, 4387–4393. [PubMed: 21346249]

Allard B, Cousineau I, Allard D, Buisseret L, Pommey S, Chrobak P, and Stagg J (2019). Adenosine A2a receptor promotes lymphangiogenesis and lymph node metastasis. Oncoimmunology 8, 1601481. [PubMed: 31413909]

Bailey-Bucktrout SL, Martinez-Llordella M, Zhou X, Anthony B, Rosenthal W, Luche H, Fehling HJ, and Bluestone JA (2013). Self-antigen-driven activation induces instability of regulatory T cells during an inflammatory autoimmune response. Immunity 39, 949–962. [PubMed: 24238343]

Bortoluzzi A, Vincenzi F, Govoni M, Padovan M, Ravani A, Borea PA, and Varani K (2016). A2A adenosine receptor upregulation correlates with disease activity in patients with systemic lupus erythematosus. Arthritis Res. Ther 18, 192. [PubMed: 27566294]

Brinkman CC, Iwami D, Hritzo MK, Xiong Y, Ahmad S, Simon T, Hippen KL, Blazar BR, and Bromberg JS (2016). Treg engage lymphotoxin beta receptor for afferent lymphatic transendothelial migration. Nat. Commun 7, 12021. [PubMed: 27323847]

Burrell BE, Nakayama Y, Xu J, Brinkman CC, and Bromberg JS (2012). Regulatory T cell induction, migration, and function in transplantation. J. Immunol 189, 4705–4711. [PubMed: 23125426]

Butcher MJ, Filipowicz AR, Waseem TC, McGary CM, Crow KJ, Magilnick N, Boldin M, Lundberg PS, and Galkina EV (2016). Atherosclerosis-driven Treg plasticity results in formation of a dysfunctional subset of plastic IFNγ+ Th1/Tregs. Circ. Res 119, 1190–1203. [PubMed: 27635087]

Chen Q, Kim YC, Laurence A, Punkosdy GA, and Shevach EM (2011). IL-2 controls the stability of Foxp3 expression in TGF-beta-induced Foxp3+ T cells in vivo. J. Immunol 186, 6329–6337. [PubMed: 21525380]

Chinen T, Kannan AK, Levine AG, Fan X, Klein U, Zheng Y, Gasteiger G, Feng Y, Fontenot JD, and Rudensky AY (2016). An essential role for the IL-2 receptor in Treg cell function. Nat. Immunol 17, 1322–1333. [PubMed: 27595233]

Comerford I, Harata-Lee Y, Bunting MD, Gregor C, Kara EE, and McColl SR (2013). A myriad of functions and complex regulation of the CCR7/CCL19/CCL21 chemokine axis in the adaptive immune system. Cytokine Growth Factor Rev. 24, 269–283. [PubMed: 23587803]

Duarte JH, Zelenay S, Bergman ML, Martins AC, and Demengeot J (2009). Natural Treg cells spontaneously differentiate into pathogenic helper cells in lymphopenic conditions. Eur. J. Immunol 39, 948–955. [PubMed: 19291701]

Fletcher AL, Malhotra D, Acton SE, Lukacs-Kornek V, Bellemare-Pelletier A, Curry M, Armant M, and Turley SJ (2011). Reproducible isolation of lymph node stromal cells reveals site-dependent differences in fibroblastic reticular cells. Front. Immunol 2, 35. [PubMed: 22566825]

Fontenot JD, Gavin MA, and Rudensky AY (2003). Foxp3 programs the development and function of CD4+CD25+ regulatory T cells. Nat. Immunol 4, 330–336. [PubMed: 12612578]

Fontenot JD, Rasmussen JP, Williams LM, Dooley JL, Farr AG, and Rudensky AY (2005). Regulatory T cell lineage specification by the forkhead transcription factor foxp3. Immunity 22, 329–341. [PubMed: 15780990]

Futterer A, Mink K, Luz A, Kosco-Vilbois MH, and Pfeffer K (1998). The lymphotoxin beta receptor controls organogenesis and affinity maturation in peripheral lymphoid tissues. Immunity 9, 59–70. [PubMed: 9697836]

Garg G, Muschaweckh A, Moreno H, Vasanthakumar A, Floess S, Lepennetier G, Oellinger R, Zhan Y, Regen T, Hiltensperger M, et al. (2019). Blimp1 prevents methylation of Foxp3 and loss

of regulatory T cell identity at sites of inflammation. Cell Rep 26, 1854–1868.e5. [PubMed: 30759395]

Gavin MA, Rasmussen JP, Fontenot JD, Vasta V, Manganiello VC, Beavo JA, and Rudensky AY (2007). Foxp3-dependent programme of regulatory T-cell differentiation. Nature 445, 771–775. [PubMed: 17220874]

Gu J, Ni X, Pan X, Lu H, Lu Y, Zhao J, Guo Zheng S, Hippen KL, Wang X, and Lu L (2016). Human CD39hi regulatory T cells present stronger stability and function under inflammatory conditions. Cell Mol. Immunol 14, 521–528.

Guo J, and Zhou X (2015). Regulatory T cells turn pathogenic. Cell Mol. Immunol 12, 525–532. [PubMed: 25942597]

Hippen KL, Merkel SC, Schirm DK, Sieben CM, Sumstad D, Kadidlo DM, McKenna DH, Bromberg JS, Levine BL, Riley JL, et al. (2011). Massive ex vivo expansion of human natural regulatory T cells (Tregs) with minimal loss of in vivo functional activity. Sci. Transl. Med 3, 83ra41.

Hua J, Inomata T, Chen Y, Foulsham W, Stevenson W, Shiang T, Bluestone JA, and Dana R (2018). Pathological conversion of regulatory T cells is associated with loss of allotolerance. Sci. Rep 8, 7059. [PubMed: 29728574]

Jacobson KA, Tosh DK, Jain S, and Gao Z-G (2019). Historical and current adenosine receptor agonists in preclinical and clinical development. Front. Cell Neurosci 13, 124. [PubMed: 30983976]

Joller N, and Kuchroo VK (2014). Good guys gone bad: exTreg cells promote autoimmune arthritis. Nat. Med 20, 15–17. [PubMed: 24398957]

Junius S, Mavrogiannis AV, Lemaitre P, Gerbaux M, Staels F, Malviya V, Burton O, Gergelits V, Singh K, Tito Tadeo RY, et al. (2021). Unstable regulatory T cells, enriched for naïve and Nrp1neg cells, are purged after fate challenge. Sci. Immunol 6, eabe4723. [PubMed: 34301799]

Komatsu N, Mariotti-Ferrandiz ME, Wang Y, Malissen B, Waldmann H, and Hori S (2009). Heterogeneity of natural Foxp3+ T cells: a committed regulatory T-cell lineage and an uncommitted minor population retaining plasticity. Proc. Natl. Acad. Sci. U S A 106, 1903–1908. [PubMed: 19174509]

Komatsu N, Okamoto K, Sawa S, Nakashima T, Oh-hora M, Kodama T, Tanaka S, Bluestone JA, and Takayanagi H (2013). Pathogenic conversion of Foxp3+ T cells into TH17 cells in autoimmune arthritis. Nat. Med 20, 62–68. [PubMed: 24362934]

Lam AJ, Uday P, Gillies JK, and Levings MK (2021). Helios is a marker, not a driver, of human Treg stability. Eur. J. Immunol 52, 75–84. [PubMed: 34561855]

Li J, McArdle S, Gholami A, Kimura T, Wolf D, Gerhardt T, Miller J, Weber C, and Ley K (2016). CCR5+ T-bet+ FoxP3+ effector CD4 T cells drive atherosclerosis. Circ. Res 118, 1540–1552. [PubMed: 27021296]

Li L, Shirkey MW, Zhang T, Xiong Y, Piao W, Saxena V, Paluskievicz C, Lee YS, Toney N, Cerel BM, et al. (2020). The lymph node stromal laminin alpha 5 shapes alloimmunity. J. Clin. Invest 130, 2602–2619. [PubMed: 32017712]

Lin W, Haribhai D, Relland LM, Truong N, Carlson MR, Williams CB, and Chatila TA (2007). Regulatory T cell development in the absence of functional Foxp3. Nat. Immunol 8, 359–368. [PubMed: 17273171]

Lio CW, and Hsieh CS (2008). A two-step process for thymic regulatory T cell development. Immunity 28, 100–111. [PubMed: 18199417]

Miyao T, Floess S, Setoguchi R, Luche H, Fehling HJ, Waldmann H, Huehn J, and Hori S (2012). Plasticity of Foxp3(+) T cells reflects promiscuous Foxp3 expression in conventional T cells but not reprogramming of regulatory T cells. Immunity 36, 262–275. [PubMed: 22326580]

Muhammad F, Wang D, McDonald T, Walsh M, Drenen K, Montieth A, Foster CS, and Lee DJ (2020). TIGIT+ A2Ar-Dependent anti-uveitic Treg cells are a novel subset of Tregs associated with resolution of autoimmune uveitis. J. Autoimmun 111, 102441. [PubMed: 32201225]

O'Brien N, Jones ST, Williams DG, Cunningham HB, Moreno K, Visentin B, Gentile A, Vekich J, Shestowsky W, Hiraiwa M, et al. (2009). Production and characterization of monoclonal anti-sphingosine-1-phosphate antibodies. J. Lipid Res 50, 2245–2257. [PubMed: 19509417]

Ochando JC, Yopp AC, Yang Y, Garin A, Li Y, Boros P, Llodra J, Ding Y, Lira SA, Krieger NR, et al. (2005). Lymph node occupancy is required for the peripheral development of alloantigen-specific Foxp3+ regulatory T cells. J. Immunol 174, 6993–7005. [PubMed: 15905542]

Ohkura N, Kitagawa Y, and Sakaguchi S (2013). Development and maintenance of regulatory T cells. Immunity 38, 414–423. [PubMed: 23521883]

Ohta A, Kini R, Ohta A, Subramanian M, Madasu M, and Sitkovsky M (2012). The development and immunosuppressive functions of CD4(+) CD25(+) FoxP3(+) regulatory T cells are under influence of the adenosine-A2A adenosine receptor pathway. Front. Immunol 3, 190. [PubMed: 22783261]

Petzold C, Steinbronn N, Gereke M, Strasser RH, Sparwasser T, Bruder D, Geffers R, Schallenberg S, and Kretschmer K (2014). Fluorochrome-based definition of naturally occurring Foxp3(+) regulatory T cells of intra- and extrathymic origin. Eur. J. Immunol 44, 3632–3645. [PubMed: 25159127]

Piao W, Xiong Y, Famulski K, Brinkman CC, Li L, Toney N, Wagner C, Saxena V, Simon T, and Bromberg JS (2018). Regulation of T cell afferent lymphatic migration by targeting LTbetaR-mediated non-classical NFkappaB signaling. Nat. Commun 9, 3020. [PubMed: 30069025]

Piao W, Xiong Y, Famulski K, Brinkman CC, Li L, Toney N, Wagner C, Saxena V, Simon T, and Bromberg JS (2019). Author Correction: regulation of T cell afferent lymphatic migration by targeting LTbetaR-mediated non-classical NFkappaB signaling. Nat. Commun 10, 2927. [PubMed: 31249309]

Piao W, Xiong Y, Li L, Saxena V, Smith KD, Hippen KL, Paluskievicz C, Willsonshirkey M, Blazar BR, Abdi R, et al. (2020). Regulatory T cells condition lymphatic endothelia for enhanced transendothelial migration. Cell Rep. 30, 1052–1062.e5. [PubMed: 31995749]

Romio M, Reinbeck B, Bongardt S, Huls S, Burghoff S, and Schrader J (2011). Extracellular purine metabolism and signaling of CD73-derived adenosine in murine Treg and Teff cells. Am. J. Physiol. Cell Physiol 301, C530–C539. [PubMed: 21593451]

Rubtsov YP, Niec RE, Josefowicz S, Li L, Darce J, Mathis D, Benoist C, and Rudensky AY (2010). Stability of the regulatory T cell lineage in vivo. Science 329, 1667–1671. [PubMed: 20929851]

Russell JM, Stephenson GS, Yellowley CE, and Benton HP (2007). Adenosine inhibition of lipopolysaccharide-induced interleukin-6 secretion by the osteoblastic cell line MG-63. Calcified Tissue Int 81, 316–326.

Sauer AV, Brigida I, Carriglio N, Hernandez RJ, Scaramuzza S, Clavenna D, Sanvito F, Poliani PL, Gagliani N, Carlucci F, et al. (2012). Alterations in the adenosine metabolism and CD39/CD73 adenosinergic machinery cause loss of Treg cell function and autoimmunity in ADA-deficient SCID. Blood 119, 1428–1439. [PubMed: 22184407]

Saxena V, Lakhan R, Iyyathurai J, and Bromberg JS (2021). Mechanisms of exTreg induction. Eur. J. Immunol 51, 1956–1967. [PubMed: 33975379]

Saxena V, Li L, Paluskievicz C, Kasinath V, Bean A, Abdi R, Jewell CM, and Bromberg JS (2019). Role of lymph node stroma and microenvironment in T cell tolerance. Immunol. Rev 292, 9–23. [PubMed: 31538349]

Simon T, Li L, Wagner C, Zhang T, Saxena V, Brinkman CC, Tostanoski LH, Ostrand-Rosenberg S, Jewell C, Shea-Donohue T, et al. (2019). Differential regulation of T-cell immunity and tolerance by stromal laminin expressed in the lymph node. Transplantation 103, 2075–2089. [PubMed: 31343575]

Srinivasan RS, Dillard ME, Lagutin OV, Lin FJ, Tsai S, Tsai MJ, Samokhvalov IM, and Oliver G (2007). Lineage tracing demonstrates the venous origin of the mammalian lymphatic vasculature. Genes Dev. 21, 2422–2432. [PubMed: 17908929]

Tomura M, Honda T, Tanizaki H, Otsuka A, Egawa G, Tokura Y, Waldmann H, Hori S, Cyster JG, Watanabe T, et al. (2010). Activated regulatory T cells are the major T cell type emigrating from the skin during a cutaneous immune response in mice. J. Clin. Invest 120, 883–893. [PubMed: 20179354]

Wan YY, and Flavell RA (2007). Regulatory T-cell functions are subverted and converted owing to attenuated Foxp3 expression. Nature 445, 766–770. [PubMed: 17220876]

Williams LM, and Rudensky AY (2007). Maintenance of the Foxp3-dependent developmental program in mature regulatory T cells requires continued expression of Foxp3. Nat. Immunol 8, 277–284. [PubMed: 17220892]

Wimmer N, Huber B, Barabas N, Rohrl J, Pfeffer K, and Hehlgans T (2012). Lymphotoxin beta receptor activation on macrophages induces cross-tolerance to TLR4 and TLR9 ligands. J. Immunol 188, 3426–3433. [PubMed: 22357629]

Xiong Y, Ahmad S, Iwami D, Brinkman CC, and Bromberg JS (2016). T-bet regulates natural regulatory T cell afferent lymphatic migration and suppressive function. J. Immunol 196, 2526–2540. [PubMed: 26880765]

Xiong Y, Brinkman CC, Famulski KS, Mongodin EF, Lord CJ, Hippen KL, Blazar BR, and Bromberg JS (2017). A robust in vitro model for translymphatic endothelial migration. Sci. Rep 7, 1633. [PubMed: 28487567]

Yang J, Cornelissen F, Papazian N, Reijmers RM, Llorian M, Cupedo T, Coles M, and Seddon B (2018). IL-7-dependent maintenance of ILC3s is required for normal entry of lymphocytes into lymph nodes. J. Exp. Med 215, 1069–1077. [PubMed: 29472496]

Zarek PE, Huang CT, Lutz ER, Kowalski J, Horton MR, Linden J, Drake CG, and Powell JD (2008). A2A receptor signaling promotes peripheral tolerance by inducing T-cell anergy and the generation of adaptive regulatory T cells. Blood 111, 251–259. [PubMed: 17909080]

Zhang N, Schroppel B, Lal G, Jakubzick C, Mao X, Chen D, Yin N, Jessberger R, Ochando JC, Ding Y, et al. (2009). Regulatory T cells sequentially migrate from inflamed tissues to draining lymph nodes to suppress the alloimmune response. Immunity 30, 458–469. [PubMed: 19303390]

Zheng X, and Wang D (2020). The adenosine A2A receptor agonist accelerates bone healing and adjusts Treg/Th17 cell balance through interleukin 6. Biomed. Res. Int 2020, 1–13.

Zhou X, Bailey-Bucktrout SL, Jeker LT, Penaranda C, Martinez-Llordella M, Ashby M, Nakayama M, Rosenthal W, and Bluestone JA (2009). Instability of the transcription factor Foxp3 leads to the generation of pathogenic memory T cells in vivo. Nat. Immunol 10, 1000–1007. [PubMed: 19633673]

Highlights

- Treg TEM across afferent lymphatic LECs is required for graft protection
- Lymphotoxin LTαβ-LTβR interactions between Treg and LECs guide Treg migration
- Disrupting Treg-LEC interactions causes Treg conversion to Foxp3^{lo}CD25^{lo} exTregs
- LTβR-NFκB-induced IL-6 promotes and adenosine-A2AR inhibits exTreg conversion

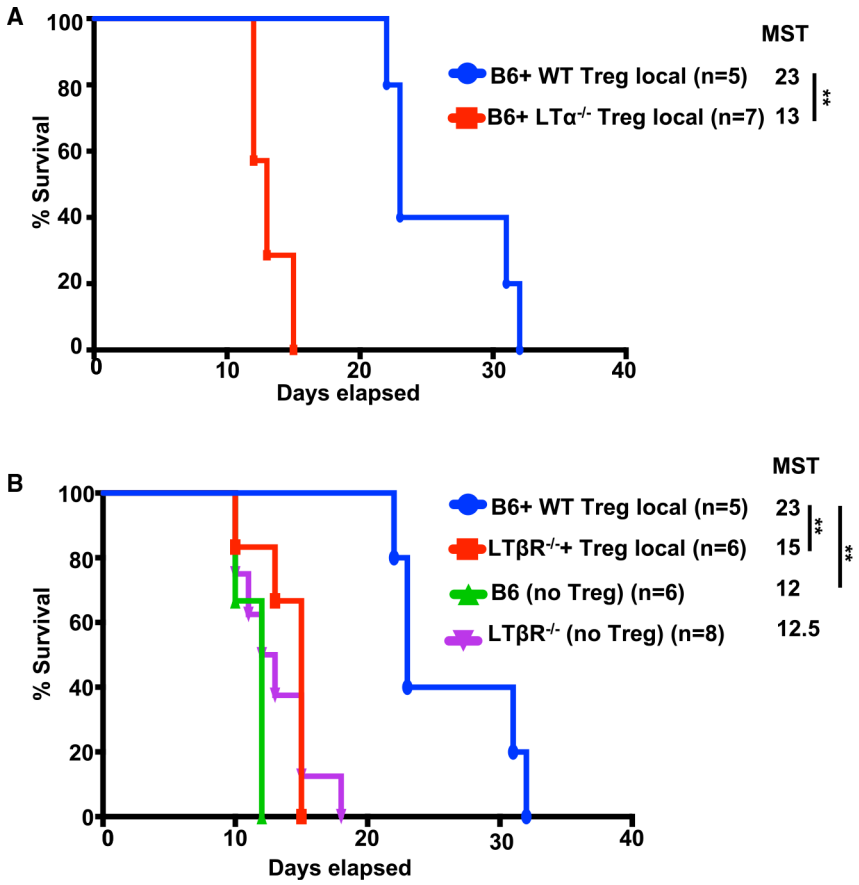

Figure 1. LTαβ-LTβR signaling pathway regulates graft survival

BALB/c islet-allograft survival in streptozotocin-induced diabetic C57BL/6 background recipients.

(A and B) C57BL/6 (B6) and (B) LTβR$^{-/-}$ recipients. 1 × 10^6 tTregs from (A) LTα$^{-/-}$ or (A and B) WT Foxp3GFP mice mixed with islets or islets alone (no Tregs).

Data pooled from 3 independent experiments with 3 recipient mice in each group. Graft survival by log rank (Mantel-Cox) test, **p < 0.01, Mean survival time (MST; days).

See also Figure S1.

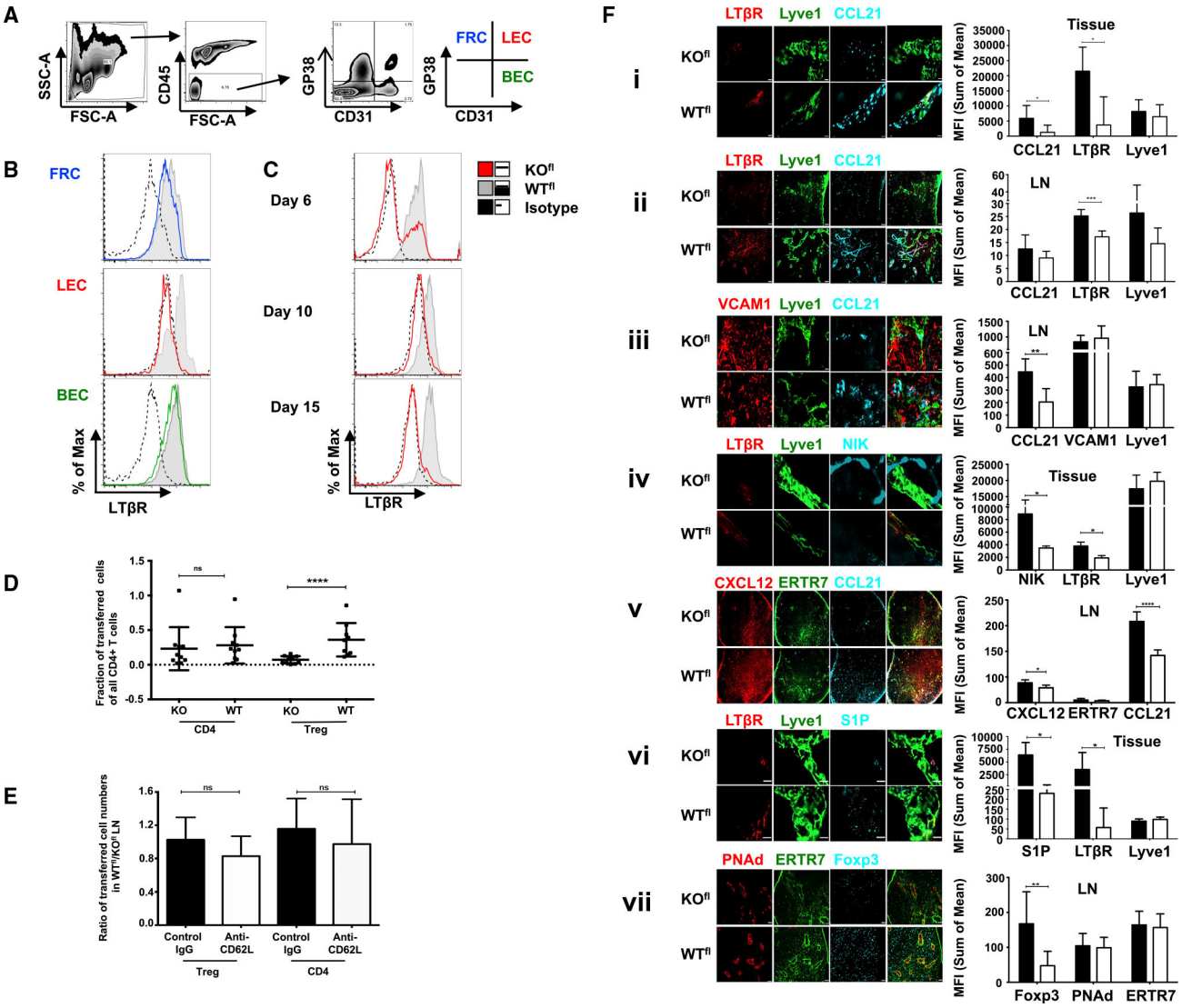

Figure 2. Conditional ablation of LTβR gene in lymphatic endothelial cells

(A–C) Prox1CreER$^{T2-/-}$LTβR$^{fl/fl}$ (WT) and Prox1CreER$^{T2+/-}$LTβR$^{fl/fl}$ (KO^{fl}) mice treated with tamoxifen (125 mg/kg intraperitoneally [i.p.]) for 5 days, and stromal cells analyzed at indicated times after the first injection. (A) Gating strategy for different stromal cell populations. (B) LTβR expression in different stromal cell populations (FRCs, fibroblastic reticular cells [CD45$^-$CD31$^-$GP38$^+$], LECs, lymphatic endothelial cells [CD45$^-$CD31$^+$GP38$^+$], and BECs, blood endothelial cells [CD45$^-$CD31$^+$GP38$^-$]) harvested from peripheral LNs 10 days after first tamoxifen injection. (C) LTβR expression on LECs harvested from peripheral LNs at indicated days after first tamoxifen injection. (B and C) Data from one experiment each for days 6 and 15 and from three experiments for day 10. (D) 1 × 10^6 sorted tTregs (CD4$^+$Foxp3GFP$^+$) or naive CD4 (CD4$^+$CD44^{lo}CD25$^-$Foxp3$^-$) cells injected into hind footpads of KO^{fl} and WT^{fl} mice at indicated times after initiation of tamoxifen treatment. Migration of indicated cells to popliteal dLNs analyzed 16 h later. (E) Ratio of adoptively transferred CD4$^+$ naive T cells and tTregs in LNs in WT^{fl} to KO^{fl} recipients. 2 × 10^7 cells containing both naive CD4$^+$ T cells plus tTregs were injected

intravenously (i.v.). Eighteen h later, recipients were treated with 100 μg anti-CD62L or control mAbs. Eighteen h after mAb treatment, LNs were harvested and analyzed by flow cytometry.

(F) Ear pinna whole-mount stains (i, iv, and vi) and immunohistochemistry (ii, iii, v, and vii) of LNs from Prox1CreER$^{T2-/-}$LTβR$^{fl/fl}$ (WT^{fl}) and Prox1CreER$^{T2+/-}$LTβR$^{fl/fl}$ (KO^{fl}) mice treated with tamoxifen and analyzed for indicated markers. Days after tamoxifen initiated: (i, iv, and vi) 16, (ii) 10, and (iii, v, and vii) 24. Bar diagrams: summary of the mean fluorescent intensity (MFI) for indicated markers.

(A–E) Data are representative of 2 experiments with 3–5 mice in each group. (F) Data are representative of 1 experiment involving 5 mice per group, with 2–3 ear pinnae or 2–3 LNs for each staining condition, and 5–10 fields/sample, acquired at 20× (scale bar, 42 μm) or 60× (scale bar, 20 μm) magnification. Error bars are SD. Student's t test. NS, not significant, *$p < 0.05$, **$p < 0.01$, ***$p < 0.001$, ****$p < 0.0001$.

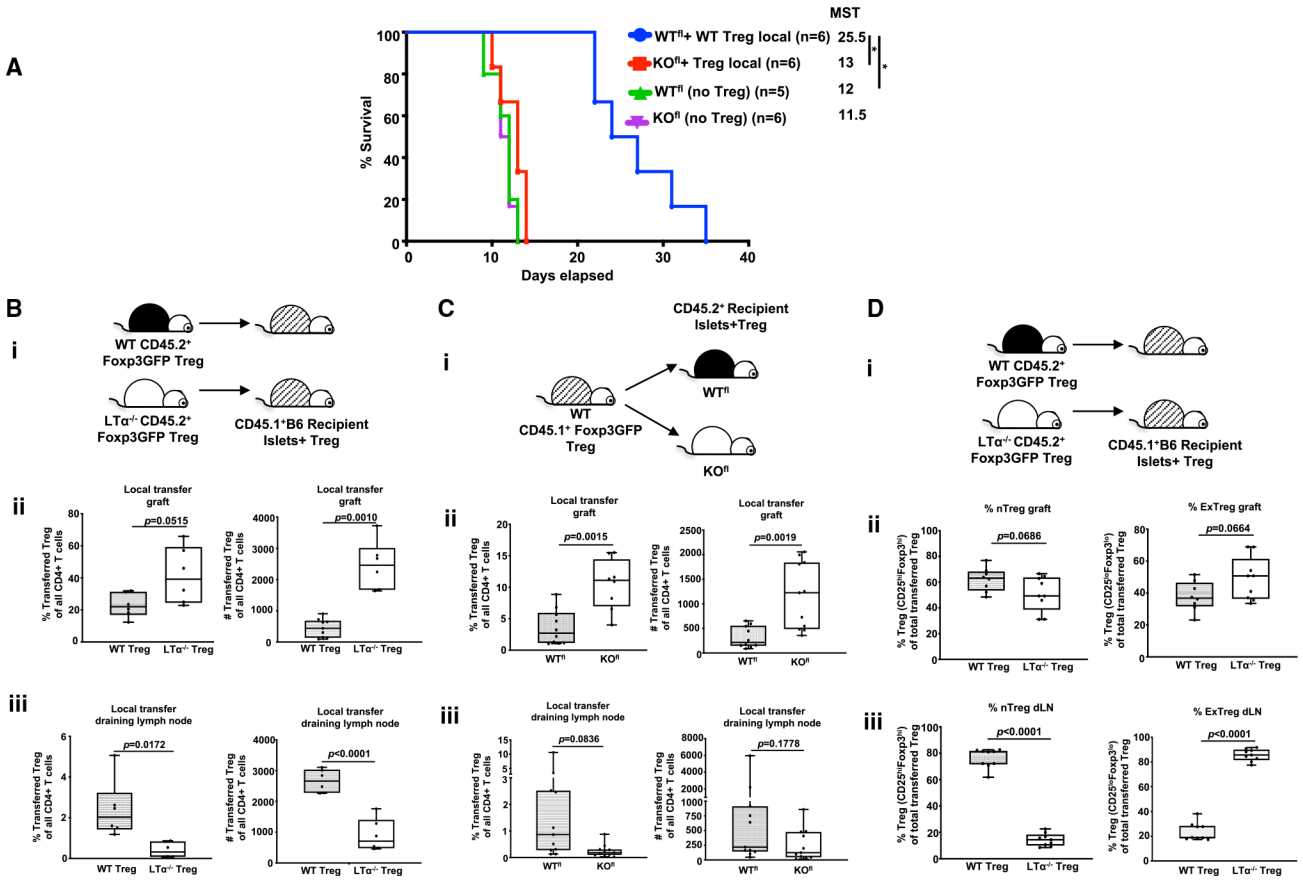

Figure 3. Treg-LTαβ and LEC-LTβR interaction regulates graft survival and Treg migration and stability

BALB/c islet-allograft survival in streptozotocin-induced diabetic C57BL/6 background recipients.

(A) WT^{fl} and KO^{fl} diabetic recipients treated with tamoxifen received 1×10^6 tTregs from WT Foxp3GFP mice mixed with islets or islets alone (no Tregs). Graft survival compared by log rank (Mantel-Cox) test; *$p < 0.05$, MST (days).

(B) 1×10^6 tTregs from WT or $LT\alpha^{-/-}$ Foxp3GFP mixed with BALB/c islets and transplanted to diabetic $CD45.1^+$ C57BL/6. Grafts and dLNs were harvested after 4 days and analyzed for Treg content by flow cytometry.

(C) 1×10^6 tTregs from $CD45.1^+$ WT Foxp3GFP mixed with islets and transplanted to diabetic, tamoxifen-treated $CD45.2^+$ WT^{fl} or KO^{fl}. Recipient mice were treated with tamoxifen and rested for 10 days before streptozotocin administration. Islet transplantation performed at least 1 week after streptozotocin treatment. Percentage and numbers of adoptively transferred Tregs in each population are measured.

(D) Cells from groups treated as in (B) analyzed for changes in Tregs. tTregs from WT or $LT\alpha^{-/-}$ Foxp3GFP plus islets transplanted to diabetic $CD45.1^+$ C57BL/6. Grafts and dLNs were harvested 4 days after transplantation. Transferred cells were analyzed for CD25 and Foxp3 expression. Average cell percentages for $CD25^{hi}Foxp3^{hi}$ tTregs and $CD25^{lo}Foxp3^{lo}$ exTregs are shown.

Data were pooled from 3 independent experiments with 3 recipient mice in each group. Errors bars are SD. Unpaired t test with Welch's correction for comparison of cell numbers and percentages.

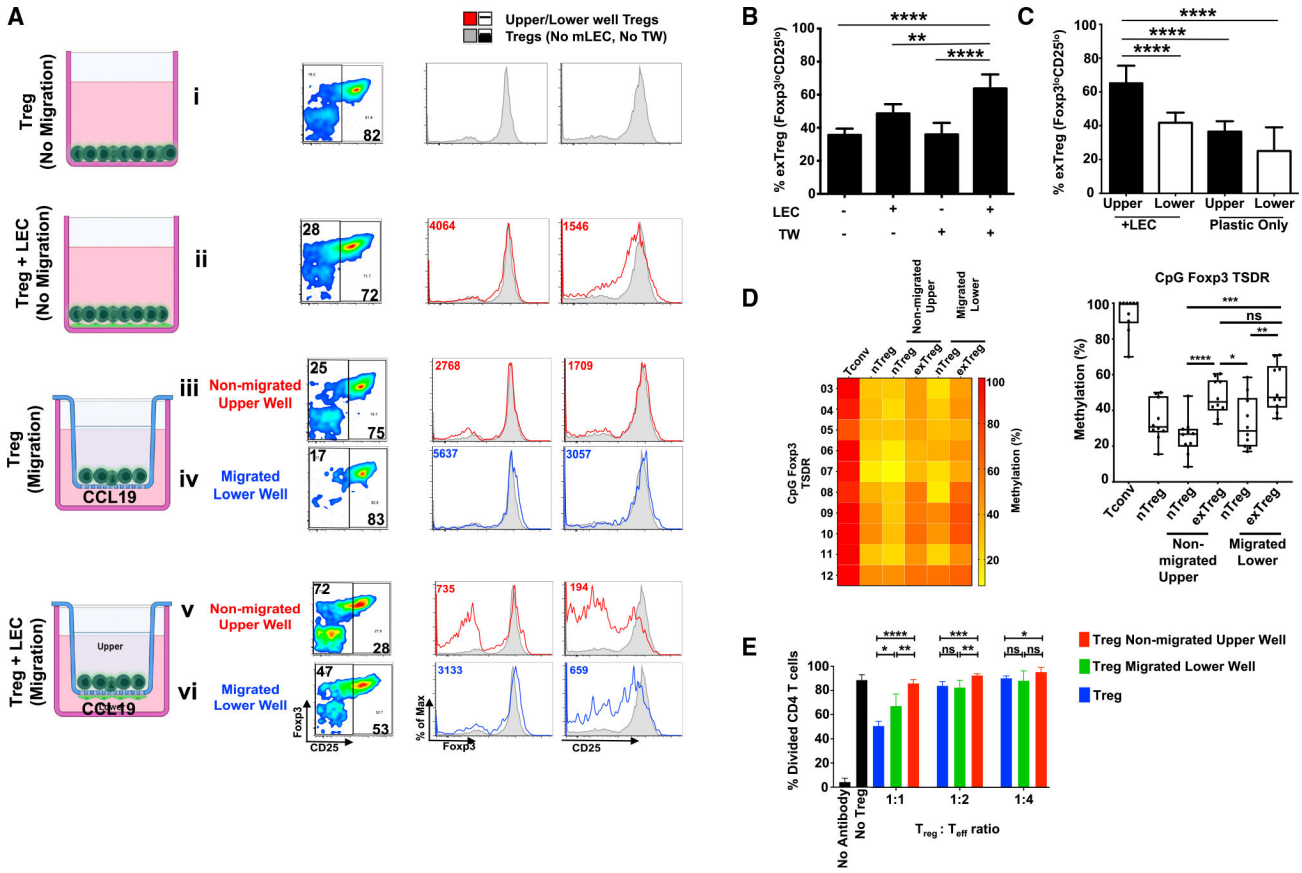

Figure 4. LTαβ-LTβR signaling regulates Treg stability, *Foxp3* demethylation state, and Treg suppression function

2×10^5 WT Foxp3GFP tTregs added to the upper well of a Boyden chamber or in a well with or without LECs. tTregs migrated or incubated for 16 h.

(A) Percentage of total CD4 cells maintaining tTreg ($CD25^{Hi}Foxp3^{Hi}$) or converting to exTreg ($CD25^{Lo}Foxp3^{Lo}$) phenotypes under indicated conditions. Histograms show expression of indicated markers by Tregs harvested from upper and lower wells.

(B) Percentage of exTregs ($CD25^{Lo}Foxp3^{Lo}$) in upper wells from indicated conditions.

(C) Percentage of exTregs ($CD25^{Lo}Foxp3^{Lo}$) from indicated wells and conditions. Data are representative of 9 independent experiments. Cells were gated on Annexin-V^{-}7-AAD^{-}/$CD4^{+}$.

(D) Tregs sorted from exTreg assay and genomic DNA analyzed for the methylation status. Data are representative of 3 independent biological replicates. Cumulative quantitation of the methylation of all the CpG islands in TSDR is shown.

(E) *In vitro* microsuppression assay showing percentage of conventional CD4 responder T cells that divided under various indicated conditions. $CD4^{+}Foxp3GFP^{+}$ cells were sorted after incubating with LECs in a Boyden chamber for 16 h and then were added to suppressor cultures. Results were pooled from triplicate wells in 3 independent experiments.

(A–C) Bar diagrams show means and SD. One-way ANOVA compares means of all groups against each other with Dunnett's multiple comparison test. (D) Repeated measures by

one-way ANOVA with Tukey's multiple comparisons test. *p < 0.05, **p < 0.01, ****p < 0.0001. (E) Student's t test.

See also Figures S2, S5, and S6.

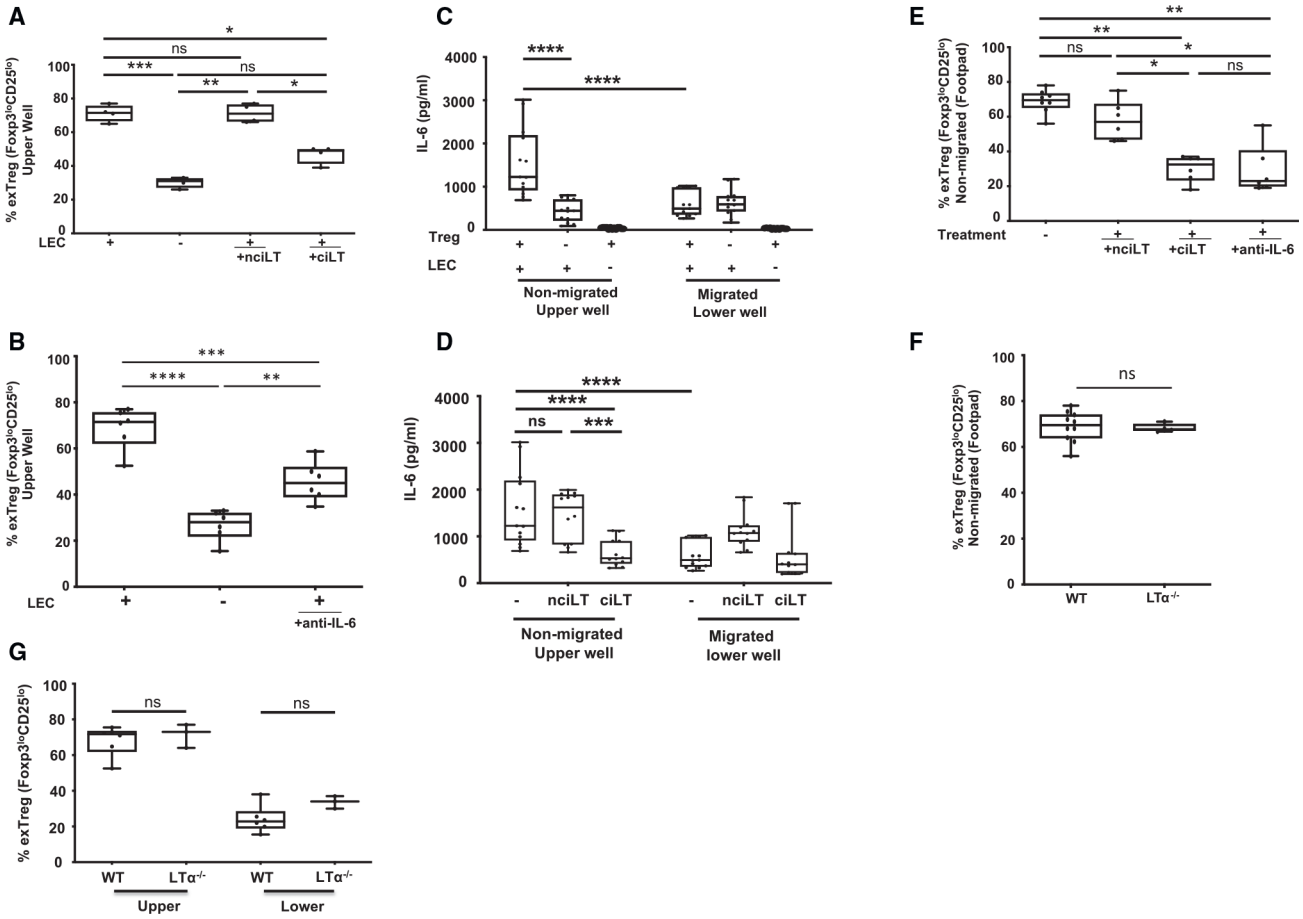

Figure 5. Treg-LEC interactions during transendothelial migration regulate Treg stability

(A, B, and G) 2×10^5 Foxp3GFP tTregs added to the upper well of a Boyden chamber or a well with or without LECs. tTregs were migrated or incubated for 16 h and analyzed from upper and lower wells. Cells were gated on Annexin-V$^-$7-AAD$^-$/CD4$^+$. Bar diagrams are a summary of 3–4 independent experiments. (A and B) LEC pre-treatment with LTβR decoy peptides (40 μM) (A), and Tregs were co-cultured with anti-IL-6 (10 μg/mL) (B).

(C) ELISA for IL-6 in the exTreg assay supernatants after 16 h culture.

(D) ELISA for IL-6 in the exTreg assay with indicated LTβR decoy peptides (40 μM); supernatants were assayed after 16 h culture.

(E and F) Sorted tTregs (CD4$^+$Foxp3GFP$^+$) injected into hind footpads of naive mice, and exTreg conversion of non-migrated Tregs in the footpads was analyzed 16 h later. The results of pooled footpads (4–6 footpads/2–3 mice) per treatment condition from 2 independent experiments are shown. (E) tTregs along with indicated LTβR decoy peptides (5 nM) or with anti-IL-6 (1 μg) injected. (F) WT or LTα$^{-/-}$ tTregs were injected.

(G) WT or LTα$^{-/-}$ tTregs were added to the upper well of a Boyden chamber and analyzed for conversion to exTregs.

Bar diagrams summarize 4–5 independent experiments. Repeated measures by one-way ANOVA with Tukey's multiple comparisons test. *$p < 0.05$, **$p < 0.005$, ***$p < 0.001$, ****$p < 0.0001$.

See also Figures S4 and S7.

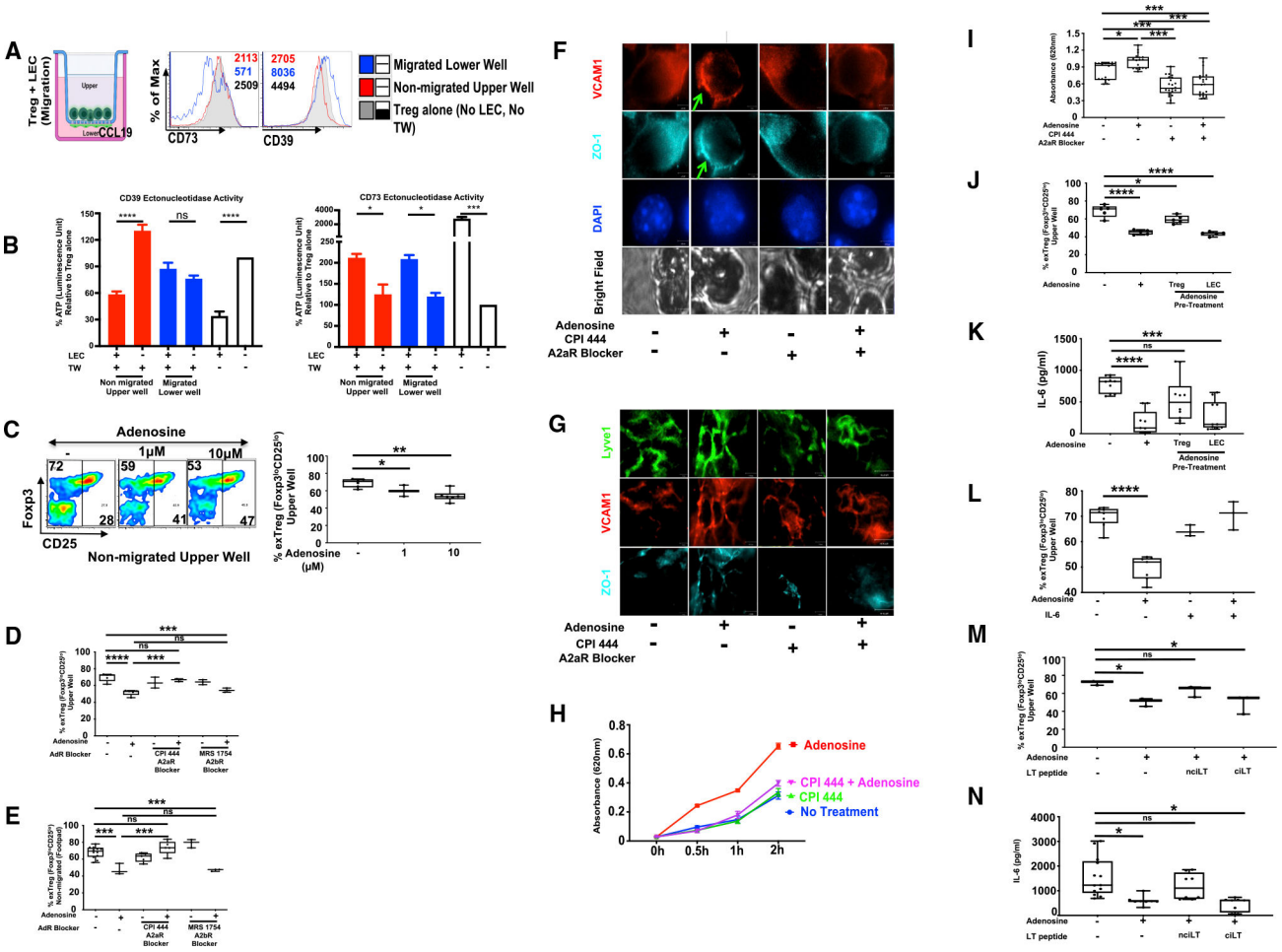

Figure 6. Adenosine regulates Treg stability

(A, C, D, and H–J) 2×10^5 Foxp3GFP tTregs added to the upper well of a Boyden chamber with or without LECs. tTregs were migrated or incubated for 16 h and analyzed from upper and/or lower wells. Cells were gated on Annexin-V$^-$7-AAD$^-$/CD4$^+$. Bar diagrams are a summary of 3–5 independent experiments. (A) Expression of indicated cell surface molecules on migrated (lower well) and non-migrated (upper well) Tregs. Numbers are geometric MFI (gMFI).

(B) Treg ectonucleotidase activity of CD39 (left panel, ATP conversion to AMP) and CD73 (right panel, consumption of AMP).

(C) Supplementation with adenosine at indicated doses prevented exTreg conversion. Representative plots and bar diagram summarizing 5 independent experiments shown.

(D) Effect of adenosine (10 μM) plus A2aR-blocker CPI 444 (1 μM) or A2bR-blocker MRS 1754 (1 μM) on inhibition of exTreg conversion.

(E) Sorted tTregs (CD4$^+$Foxp3GFP$^+$) injected into hind footpads of naive mice along with indicated adenosine receptor blocker (1 μM) with or without adenosine. exTreg conversion of non-migrated Tregs in the footpads was analyzed 16 h later.

(F and G) Effect of adenosine and/or A2aR-blocker CPI 444 pre-treatment on (F) a LEC monolayer grown on inverted Boyden chamber or on (G) mouse ears pretreated first with an A2aR blocker for 1 h and then adenosine for 4 h. Data are representative of 3 independent

experiments involving 3 mice per group, with 2–3 ear pinnae for each staining condition, and 5–10 fields/sample, acquired at 20× (scale bar, 42 μm) or 60× (scale bar, 20 μm) magnification.

(H) LEC monolayer pre-treated, as in (F), and analyzed for dye permeability.

(I) Mouse footpads injected with A2aR blocker and 1 h later with adenosine. Four h after adenosine, Evans blue dye was administered, and 16 h later, dye transport from dLNs was measured for indicated conditions.

(J and K) Effect of adenosine pre-treatment of Tregs or LECs on (J) inhibition of exTreg conversion and (K) IL-6 secretion. Results were pooled from duplicate wells in 5 independent experiments.

(L) Effect of supplementation with adenosine and/or IL-6 (10 ng/mL) on exTreg conversion in the upper chamber.

(M and N) Effect of LEC pre-treatment with LTβR decoy peptides (40 μM) on adenosine inhibition of (M) exTreg conversion and (N) IL-6 secretion.

(B–D, G, and I–N) Bar diagrams summarize 2–5 independent experiments. (E and I) Results of pooled footpads (6–12 footpads/3–6 mice) per treatment condition from 2 (I) to 3 (E) independent experiments. Repeated measures by one-way ANOVA with Tukey's multiple comparisons test. *$p < 0.05$, **$p < 0.005$, ***$p < 0.001$, ****$p < 0.0001$.

See also Figures S3, S4, S8, and S9.

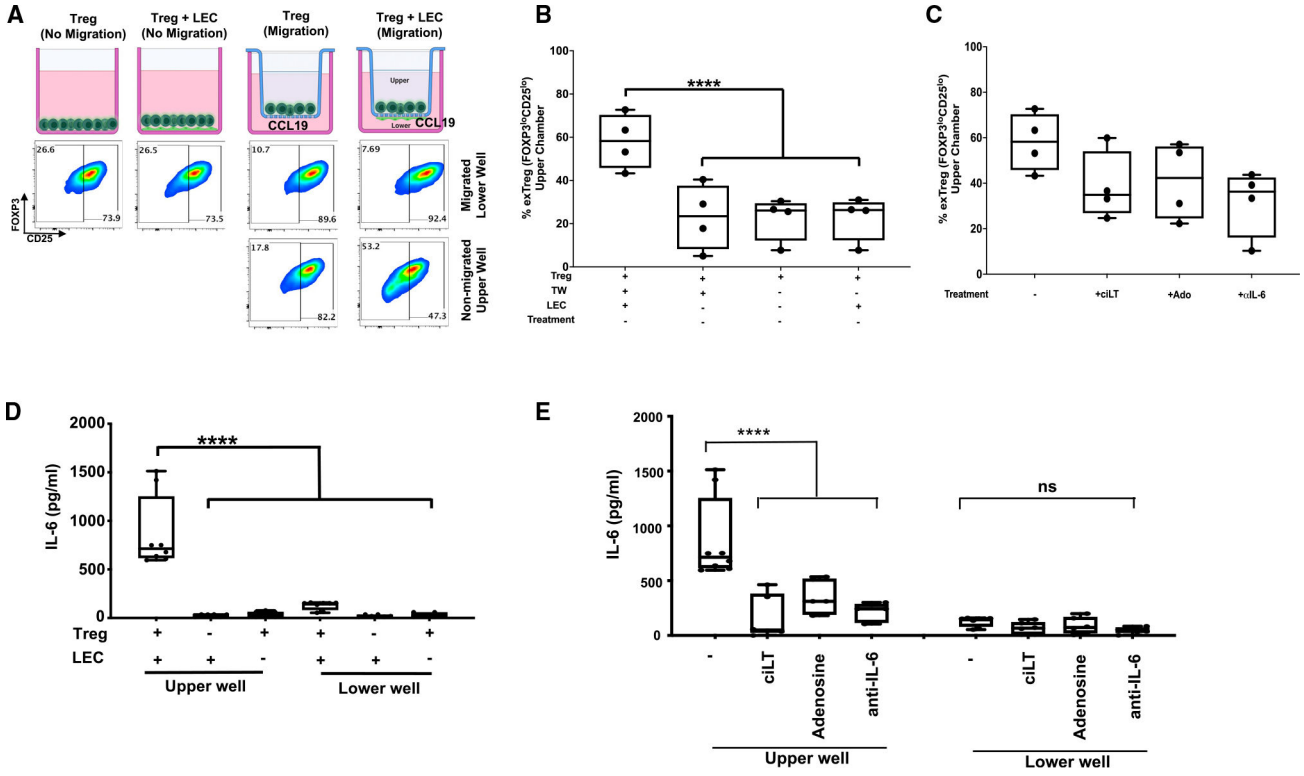

Figure 7. Human Treg-LEC interactions during TEM regulate Treg stability

5×10^4 human tTregs added to the upper well of a Boyden chamber or a well with or without primary human LECs. tTregs were migrated or incubated for 16 h and analyzed from upper and lower wells. Cells were gated on FSC-A^+SSC-A^+/$CD4^+$.

(A) Diagram of experimental groups, and dot plots from flow cytometry analysis of CD4 T cells converting to exTregs ($CD25^{Lo}FOXP3^{Lo}$) or maintaining tTreg ($CD25^{Hi}Foxp3^{Hi}$) phenotypes for one T cell donor. Numbers in the inset represent percentage of cells.

(B and D) Summary of percentage of exTregs ($CD25^{Lo}FOXP3^{Lo}$) in upper wells from indicated conditions.

(C and E) Summary of IL-6 content of supernatants. LEC pre-treatment with LTβR decoy peptide ciLT (40 μM) or co-culture with adenosine (10 μM) or anti-IL-6 (10 μg/mL).

(B–E) Summary of 4 independent donors in 2 independent experiments. Repeated measures by one-way ANOVA with Tukey's multiple comparisons test. ns $p \geq 0.05$, *$p < 0.05$, **$p < 0.01$, ***$p < 0.001$, ****$p < 0.0001$.

See also Figure S7.

KEY RESOURCES TABLE

REAGENT or RESOURCE	SOURCE	IDENTIFIER
Antibodies		
Anti-CD39 (clone 390)	BD Bioscience	Cat# 558738; RRID: AB_397097
Anti-CD16/32 (clone 93)	eBioscience	Cat# 14-0161-82; RRID: AB_467133
Anti- LTbR (FC, IHC) (clone eBio3C8)	eBioscience	Cat# 12-5671-82; RRID: AB_2016713
Anti-GP38 (clone eBio8.1.1)	eBioscience	Cat# 25-5381-80; RRID: AB_2573459
Anti-Lyve1 (FC) (clone ALY7)	eBioscience	Cat# 50-0443-82; RRID: AB_10597449
Anti-Lyve1 (IHC) (polyclonal)	Fitzgerald	Cat# 70R-LR003; RRID: AB_1287923
Anti-CD3ε (IHC) (polyclonal)	Abcam	Cat# ab49943; RRID: AB_868900
Anti-ERTR7 (IHC) (clone 73355)	Santa Cruz	Cat# SC-73355; RRID: AB_1122890
Anti-Foxp3 (FC, IHC) (clone NRRF-30)	eBioscience	Cat# 14-4771-80; RRID: AB_529583
Anti-B220 (IHC) (clone RA3-6B2)	eBioscience	Cat# 17-0452-82; RRID: AB_469395
Anti-CCL21 (IHC) (polyclonal)	R&D Systems	Cat# AF457; RRID: AB_2072083
Anti-NIK (IHC) (clone A-12)	Santa Cruz	Cat# sc-8417; RRID: AB_628021
Anti-CD45 (FC) (clone 30-F11)	eBioscience	Cat# 48-0451-82; RRID: AB_1518806
Anti-S1P (IHC) (clone LT1002)	Gift from Roger A. Sabbadini	(O'Brien et al., 2009)
Anti-ICAM-1 or Anti-CD54 (IHC) (clone YN1/1.7.4)	BioLegend	Cat# 116109; RRID: AB_313700
Anti-VCAM-1 or Anti-CD106 (IHC) (clone 429)	BioLegend	Cat# 105708; RRID: AB_313209
Anti-CCL9/mip-3β (IHC) (polyclonal)	R&D Systems	Cat# AF880; RRID: AB_2071545
Anti-CD11c (IHC) (clone HL3)	BD Bioscience	Cat# 550283; RRID: AB_393578
Anti-PNAd (IHC) (clone MECA-79)	BD Bioscience	Cat# 553863; RRID: AB_395099
Anti-PDCA1 (IHC) (clone eBio927)	eBioscience	Cat# 51-3172-82; RRID: AB_763422
Anti-CD73 (FC) (clone TY/11.8)	BioLegend	Cat# 127209; RRID: AB_11219400
Anti-CD73 (Blocking) (clone TY/23)	BD Bioscience	Cat# 550738; RRID: AB_393857
Anti-IL-10 (FC) (clone JES5-16E3)	eBioscience	Cat# 17-7101-81; RRID: AB_469501
Anti-TGFβ (FC) (clone TW7-20B9)	BioLegend	Cat# 141305; RRID: AB_10717505
Anti-Perforin (FC) (clone S16009A)	BioLegend	Cat# 154303; RRID: AB_2721462
Anti-CTLA4 or Anti-CD152 (FC) (clone UC10-4B9)	BioLegend	Cat# 106305; RRID: AB_313254
Anti-CTLA4 or Anti-CD152 (Blocking) (clone 9H10)	BioLegend	Cat# 106211; RRID: AB_2813939
Anti-GITR or Anti-CD357 (FC) (clone DTA-1)	BioLegend	Cat# 126311; RRID: AB_2271858
Anti-GITR or Anti-CD357 (Blocking) (clone 5F1)	BioLegend	Cat# 147404; RRID: AB_2563490
Anti-PD-1 or Anti-CD279 (FC) (clone J43)	eBioscience	Cat# 12-9985-81; RRID: AB_466294
Anti-PD-L1 or Anti-CD274 (FC) (clone MIH5)	eBioscience	Cat# 25-5982-80; RRID: AB_2573508
Anti-CD25 (FC) (clone PC16)	BioLegend	Cat# 102012; RRID: AB_312861
Anti-CD69 (FC) (clone H1.2F3)	BD Bioscience	Cat# 553237; RRID: AB_394726
Anti-CD39 (FC) (clone Duha59)	BioLegend	Cat# 143811; RRID: AB_2750321
Anti-CD39 (Blocking) (clone 5F2)	BioLegend	Cat# 135702; RRID: AB_2099922
Anti-Ly6G (Gr-1) (FC) (clone RB6-8C5)	eBioscience	Cat# 11-5931-82; RRID: AB_465314
Anti-CD19 (FC) (clone 1D3)	eBioscience	Cat# 11-0193-82; RRID: AB_657666
Anti- TCRγδ (FC) (clone GL3)	eBioscience	Cat# 11-5711-82; RRID: AB_465238
Anti- TCRVβ3 (FC) (clone KJ25)	BD Bioscience	Cat# 553208; RRID: AB_394708

REAGENT or RESOURCE	SOURCE	IDENTIFIER
Anti-CD3ε (FC) (clone 145-2C11)	eBioscience	Cat# 11-0031-85; RRID: AB_464883
Anti-CD11b (FC) (clone M1/70)	eBioscience	Cat# 11-0112-81; RRID: AB_464934
Anti-Ly-76 (FC) (clone TER-119)	eBioscience	Cat# 11-5921-82; RRID: AB_465311
Anti- NK1.1 (Ly-55) (FC) (clone PK136)	eBioscience	Cat# 11-5941-82; RRID: AB_465318
Anti-CD11c (FC) (clone HL3)	BD Bioscience	Cat# 553801; RRID: AB_395060
Anti-F4/80 (FC) (clone BM8)	eBioscience	Cat# 11-4801-81; RRID: AB_2735037
Anti-CD49b (FC) (clone DX5)	BD Bioscience	Cat# 553857; RRID: AB_395093
Anti-CD49b (Blocking) (clone HMa2)	BD Bioscience	Cat# 553857; RRID: AB_395093
Anti-IL-7Rα (FC) (clone A7R34)	eBioscience	Cat# 12-1271-81; RRID: AB_465843
Anti-GATA3 (FC) (clone TWAJ)	eBioscience	Cat# 46-9966-42; RRID: AB_10804487
Anti- RORγT (FC) (clone B2D)	eBioscience	Cat# 17-6981-82; RRID: AB_2573254
Anti- Thy1.1 (CD90.1) (FC) (clone HIS51)	eBioscience	Cat# 48-0900-82; RRID: AB_1272254
Anti-IL-6 (Blocking) (MP5-20F3)	BioXCell	Cat# BE0046; RRID: AB_1107709
Anti-Granzyme A (FC) (clone 3G8.5)	BioLegend	Cat# 149703; RRID: AB_2565309
Anti-Granzyme B (FC) (clone GB11)	BioLegend	Cat# 515405; RRID: AB_2294995
Anti-T-bet (FC) (clone 4B10)	BioLegend	Cat# 644809; RRID: AB_2028583
Anti- IFNγ (FC) (clone XMG1.2)	BD Bioscience	Cat# 560660; RRID: AB_1727533
Anti- ZO-1 (IHC) (clone ZO1-1A12	Thermo Fisher Scientific	Cat# 33-9100; RRID: AB_2533147
Anti- NF-kB2 anti-p100/p52 (WB) (polyclonal)	Cell Signaling	Cat# 4882; RRID: AB_10695537
Anti- Phospho-NF-kB p65 (Ser536) (WB) (clone 93H1	Cell Signaling	Cat# 3033; RRID: AB_331284
Anti-GAPDH (WB) (clone 14C10	Cell Signaling	Cat# 2118; RRID: AB_561053
Anti-CD62L (Blocking) (clone mel-14	BioXCell	Cat# BE0021; AB_1107665
Anti-Rat IgG2a (Blocking) (clone 2A3)	BioXCell	Cat# BE0089; AB_1107769
Anti-human CD25 (FC) (cloneBC96)	BioLegend	Cat# 302631; RRID: AB_11123913
Anti-human CD4 (FC) (clone OKT4)	BioLegend	Cat# 317431; RRID: AB_2028494
Anti-human FOXP3 (FC) (clone FJK-16s)	eBioscience	Cat# 11-5773-82; RRID: AB_465243
Rat IgG1 (MOPC21)	BioXCell	Cat# BE0083; RRID: AB_1107784
LTβRIg	Biogen Idec	Gift; RRID: N/A
Anti-human IL-6 (FC) (clone 6708)	R&D Systems	Cat# MAB206; RRID: N/A
Anti-Rabbit IgG Alexa Flour 647	Invitrogen	Cat# 1013785; RRID: N/A
Anti-Rabbit IgG Alexa Flour 546	Jackson ImmunoResearch	Cat# 705-546-147; RRID: AB_2340430
Anti-Rabbit IgG Alexa Flour 488	Jackson ImmunoResearch	Cat# 711-545-152; RRID: AB_2313584
Anti-Rat IgG Alexa Flour 647	Jackson ImmunoResearch	Cat# 712-605-153; RRID: AB_2340694
Anti-Rat IgG Cy3	Jackson ImmunoResearch	Cat# 712-165-153; RRID: AB_2340667
Anti-Goat IgG Cy3	Jackson ImmunoResearch	Cat# 705-165-003; RRID: AB_2340411
Anti-Goat IgG Alexa Flour 647	Jackson ImmunoResearch	Cat# 705-605-003; RRID: AB_2340436
Anti-Mouse IgG Alexa Flour 647	Jackson ImmunoResearch	Cat# 715-605-150; RRID: AB_2340862
Chemicals, peptides, and recombinant proteins		
Dynabeads	Gibco	Cat# 11452D; RRID: N/A
Recombinant CCL19	R&D Systems	Cat# 440-M3-025; RRID: N/A
Recombinant mouse IL-2	eBioscience	Cat# 14-8348-62; RRID: N/A

REAGENT or RESOURCE	SOURCE	IDENTIFIER
Cell Proliferation Dye eFluor-670	eBioscience	Cat# 65-0840-85; RRID: N/A
Collagenase D	Roche	Cat# 11088866001; RRID: N/A
Collagenase P	Roche	Cat# 11213857001; RRID: N/A
Tamoxifen	Sigma-Aldrich	Cat# T5648-1G; RRID: N/A
Streptozocin	Sigma-Aldrich	Cat# S0130-1G; RRID: N/A
Dispase	Gibco	Cat# 17105041; RRID: N/A
DNase I	Invitrogen	Cat# 18068015; RRID: N/A
Adenosine	Tocris	Cat# 3624; RRID: N/A
CPI-444	Enzo	Cat# BV-B1970; RRID: N/A
MRS-1754	Sigma	Cat# M6316; RRID: N/A
Critical commercial assays		
Mouse CD4+ T cell isolation kit	StemCell Technologies	Cat# 19852; RRID: N/A
PE Annexin V apoptosis detection kit	BD Biosciences	Cat# 559763; RRID: N/A
EZ DNA Methylation-Direct™ Kit	Zymo Research	Cat# D5020; RRID: N/A
AMP-Glo assay	Promega	Cat# V5011; RRID: N/A
ELISA MAX™ Deluxe Set Mouse IL-6	BioLegend	Cat# 431104; RRID: N/A
ELISA MAX™ Deluxe Set Human IL-6	BioLegend	Cat# 430504; RRID: N/A
Adenosine Assay Kit (Fluorometric)	Abcam	Cat# ab211094; RRID: N/A
Experimental models: Cell lines		
Primary mouse dermal LEC	Cell Biologics, Inc.	Cat# C57-6064L; RRID: N/A
Primary human dermal LEC	Cell Biologics, Inc.	Cat# H-6064L; RRID: N/A
Experimental models: Organisms/Strains		
Mouse: C57BL/6J WT	The Jackson Laboratory	Cat# JAX: 000664; RRID: IMSR_JAX:000664
Mouse: B6.SJL-Ptprc^{a} Pepc^{b}/Boyj (CD45.1)	The Jackson Laboratory	Cat# JAX: 002014; RRID: IMSR_JAX:002014
Mouse: B6.129S2-Lta^{tm1Dch}/J	The Jackson Laboratory	Cat# JAX: 002258; RRID: IMSR_JAX:002258
Mouse: C57BL/6J_Foxp3GFP	Gift	(Fontenot et al., 2005)
Mouse: C57BL/6J_ LTβR$^{fl/fl}$	Gift	(Wimmer et al., 2012)
Mouse: C57BL/6J_ Prox1 -Cre-ER^{T2}	Gift	(Srinivasan et al., 2007)
Mouse: C57BL/6J_ Prox1 -Cre-ER^{T2}-LTpR$^{fl/fl}$		This study
Mouse: C57BL/6J_ Foxp3GFP-CD45.1		This study
Mouse: C57BL/6J_ LT$\alpha^{-/-}$Foxp3GFP		This study
Software and algorithms		
Volocity 6.3	Quorum Technologies	http://quorumtechnologies.com/
FlowJo v9.9.6	TreeStar	https://www.flowjo.com
Prism 9	GraphPad Software, Inc	https://www.graphpad.com
PyroMark CpG SW 1.0.11 software	Qiagen	https://www.qiagen.com